

1 Probabilistic Assessment of Port Operation Downtimes Under Climate Change

2
3 P. Camus, A. Tomás, G. Díaz-Hernández, B. Rodríguez, C. Izaguirre, I. J. Losada

4 Affiliation for all authors. *Environmental Hydraulics Institute, Universidad de Cantabria - Avda.*
5 *Isabel Torres, 15, Parque Científico y Tecnológico de Cantabria, 39011, Santander, Spain*

6
7 Corresponding author: Paula Camus (camusp@unican.es)
8
9
10
11

12 Abstract

13 Disruptions in harbor operations have significant implications for local, regional and global
14 economies due to ports strategic role as part of the supply chain. A probabilistic evaluation of port
15 operations considering the influence of climate change is required in order to secure optimal
16 exploitation during their useful life. Here, we propose a hybrid statistic-dynamical framework
17 combining a weather generator and a metamodel. The stochastic generator is based on weather
18 types to project climate variability on hourly multivariate dependent climate drivers outside ports.
19 The metamodel efficiently transforms hourly sea conditions from the entrance of the harbor
20 towards the inside port adding the advantages of a physical process model. Thousands of hourly
21 synthetic time series based on present climate conditions and future ones were transferred inside
22 the port to perform a probabilistic analysis of port operations. Future forcing conditions were
23 defined adding several sea level rise (SLR) scenarios, sampled from their probability distribution,
24 to the synthetic sea level fluctuation time series. Wave amplification due to non-linear interactions
25 between wave and sea level variations and changes in the reflection coefficients inside the port
26 induced by SLR were modelled. Probabilistic future changes of operation downtimes were
27 quantified considering the uncertainty associated with the historical forcing conditions outside the
28 port and likely SLR scenarios. The methodology was applied to a specific case study on a regional
29 port located in the north coast of Spain, where port operability due to wave agitation was assessed.

37 **1 Introduction**

38 Port infrastructure is strategic for local, regional and global economic growth and development.
39 They play a crucial role as transportation hubs and gateways for the vast majority of goods
40 transported around the world, linking local and national supply chains to global markets.
41 Moreover, demands on ports are likely to grow in the light of expected increases in world freight
42 volumes, due to shipping efficiency and its smaller carbon footprint compared to other modes of
43 transport [1]. Other economic activities, including industry, tourism and fisheries, also flourish
44 around seaports. Thus, any significant disruption in the logistics of seaports can have significant
45 economic implications [2]. Service disruptions alone can cause considerable economic losses in
46 the order of billions of dollars and may have important second-order consequences, not only for
47 regional economies and the quality of life of those who depend directly on the port's functionality,
48 but also for the operation of global supply-chains [3].

49 Due to the type of businesses held around them, seaports are located in one of the most vulnerable
50 areas to climate change impacts, i.e. coastal areas susceptible to sea level rise and increased storm
51 intensity and/or mouths of rivers susceptible to flooding [1]. Despite this, attention to climate-
52 related impacts in ports is relatively recent [4]. The first international benchmark studies consisted
53 of an analysis of the most vulnerable to climate change port cities in 2070 [5] based on population
54 and asset exposure to water levels defined as one hundred year storm surge, and a worldwide
55 survey sent to Port Authorities to detect sectorial perceptions regarding port risks due to climate
56 change [1], respectively.

57 The first step in the evaluation of climate change impacts on ports involves reviewing all potential
58 impacts and identifying the main marine variables and the databases available where this
59 information is included [6]. Sea-level rise used to be the only climate-driver considered in the
60 assessment of climate change impacts, as for example, in the methodology proposed to map
61 vulnerability of port assets to sea-level rise relative to their location [2]. Future wave and storm
62 surge conditions are not available from Global Circulation Models (GCMs) for different
63 Representative Concentration Pathway (RCP) scenarios which are the primary tool for
64 investigating the evolution of the climate system over this century. Therefore, a downscaling
65 approach is required to obtain such future projections in order to take them into account when
66 assessing the impact of climate change in ports. The assessment of climate change effects on port
67 operability (wave agitation) has been already explored considering changes in waves using various
68 Regional Circulation Models (RCMs) for an A1B scenario [7], or by adding the effect of sea level
69 rise (SLR) in combination with wave changes for one GCM for RCP8.5 [8]. Another example is
70 the simplified approach presented in [9] to assess impacts on port operation due to overtopping at
71 the regional scale. This approach consists of a direct statistical weather-typing downscaling of
72 impact indicators (e.g., number of hours per year with overtopping exceeding a certain threshold),
73 integrating changes in storminess including waves, storm surge and sea level rise. One of the
74 advantages of this statistical downscaling method is that it allows quantifying the uncertainty
75 associated to different scenarios and climate models (30 GCMs for 2 RCPs were projected), which
76 is not possible if only one or a limited number of GCMs or RCMs are considered.

77 Climate drivers for evaluating infrastructure reliability or port operability are defined outside the
78 port, before local nearshore processes such as breaking, diffraction, or reflection have taken place.
79 Each hourly set of multivariate marine conditions at the entrance of the harbor has to be propagated
80 inside the port using a wave model at high spatial resolution. When climate change is assessed to
81 provide useful information for developing effective adaptation strategies, thousands of different

82 combinations of future forcing variables must be simulated to account for the cascading
83 uncertainty associated with the various scenarios and global/regional models [10]. This multi-scale
84 modelling approach is unaffordable computationally. However, a wide variety of metamodels have
85 been proposed to run wave models for large data sets within a reasonable computational time.
86 Metamodels are, in essence, simplified (and hence computationally efficient) representations of
87 computationally intensive models [11]. The traditional approach is to develop a ‘look-up table’
88 which involves running the model for a subset of events defined over a regular grid with a coarse
89 resolution to limit the number of simulations. Two approaches with a different degree of
90 complexity can be applied to predict the results for additional events: selecting the result of the
91 most similar design point as representative of the new event [8], or using linear interpolation
92 techniques. More sophisticated methods are developed based on the combination of a selection
93 algorithm and radial basis functions [12]. This method has been proved to be quite efficient [13]
94 since it represents the selected input boundary conditions properly and proposes a powerful
95 interpolation technique. Another alternative which doesn’t involve numerical simulations consists
96 of applying artificial neural networks to assess port operability [14], but it requires instrumental
97 data outside and inside the port.

98 To assess the safety, serviceability and exploitation of port operations, Spanish Recommendations
99 for Maritime Structures (ROM 0.0-0.1, [15]) propose a Level III Verification Method based on
100 Monte Carlo methods for the probabilistic evaluation of failure modes and operational stoppage
101 modes (downtime) of maritime structures. Modes of failure or operability are determined by non-
102 linear interactions of multiple meteo-oceanic dynamics (e.g., astronomical tide, storm surge,
103 waves), climate drivers (waves and storm surge) being statistically dependent due to a common
104 synoptic-scale atmospheric circulation generation. It is therefore necessary to use simulation
105 methodologies that address the dependency among variables. There is a wide range of multivariate
106 statistical models that have been applied to marine conditions. Depending on the type of outputs
107 they provide, models can be divided into two categories: 1) extreme events such as unconditional
108 approaches ([16], [11]); copula methods ([17], [18], [19]); weather-type based models [20] and 2)
109 time series using autoregressive models ([21], [22], [23]). The use of Monte-Carlo methods for
110 probabilistic analyses demands a high computational effort to assess infrastructure failure modes
111 or port operability. The process is even more complex if the probabilistic verification is also
112 performed including climate change projections.

113 To our knowledge, only one study has evaluated the effect of climate change in port operability
114 caused by wave agitation due to SLR (three values) and wave changes from one GCM. A
115 metamodel based on the 40 simulations of wave propagation inside the port was applied [8].
116 Inoperability time was obtained as the sum of the frequencies of occurrence from the wave sets
117 exceeding a fixed threshold. No assessment of port operation downtimes due to wave agitation has
118 been performed using a Monte-Carlo approach, nor including climate change.

119 In this work, we propose an integrated methodology for very long-term probabilistic assessments
120 of port operability due to wave agitation, including the potential effects of climate change. Only
121 port operability due to wave agitation was considered in order to simplify the methodology’s
122 description, but the method can be easily extended/used for other applications. The probabilistic
123 verification comprises the use of: 1) a stochastic generator which simulates synthetic multivariate
124 forcing conditions at the entrance of the harbor; and 2) a metamodel to transfer these marine
125 conditions inside the port. Synthetic hourly conditions of wave agitation under present and future
126 climate conditions were evaluated to obtain a probabilistic characterization of port operability and

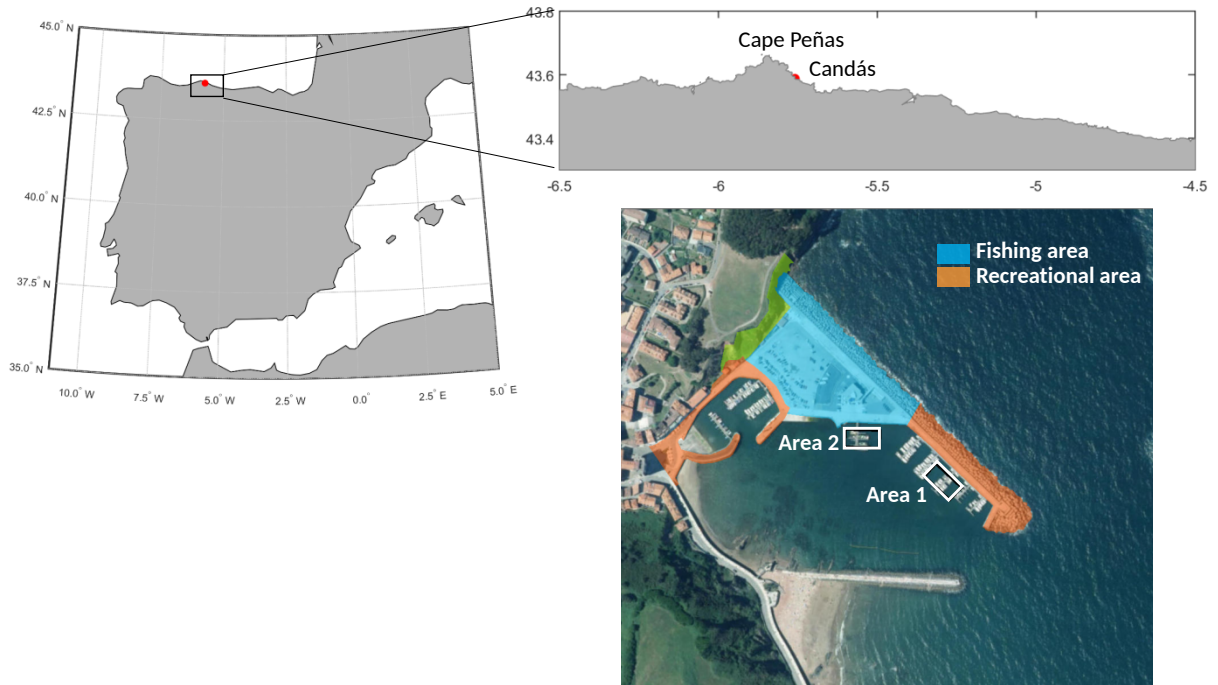
127 to assess changes due to climate change. Probabilistic sea level rise (SLR) scenarios were
128 considered to account for SLR uncertainty in the evaluation of future operation downtimes. The
129 application of the methodology was particularized to a regional fishing port currently experiencing
130 recurrent downtimes.

131 The paper is organized as follows: section 2 describes the study area used as a pilot case; section
132 3 presents the databases required for the application of the methodology and section 4 provides
133 extensive details on the overall methodology which combines a weather generator and a
134 metamodel and describes the impact of climate change on port operations. The application of the
135 methodology to the regional port is presented throughout sections 2–4. Finally, section 5
136 summarizes and concludes the work.

137

138 **2 Study area**

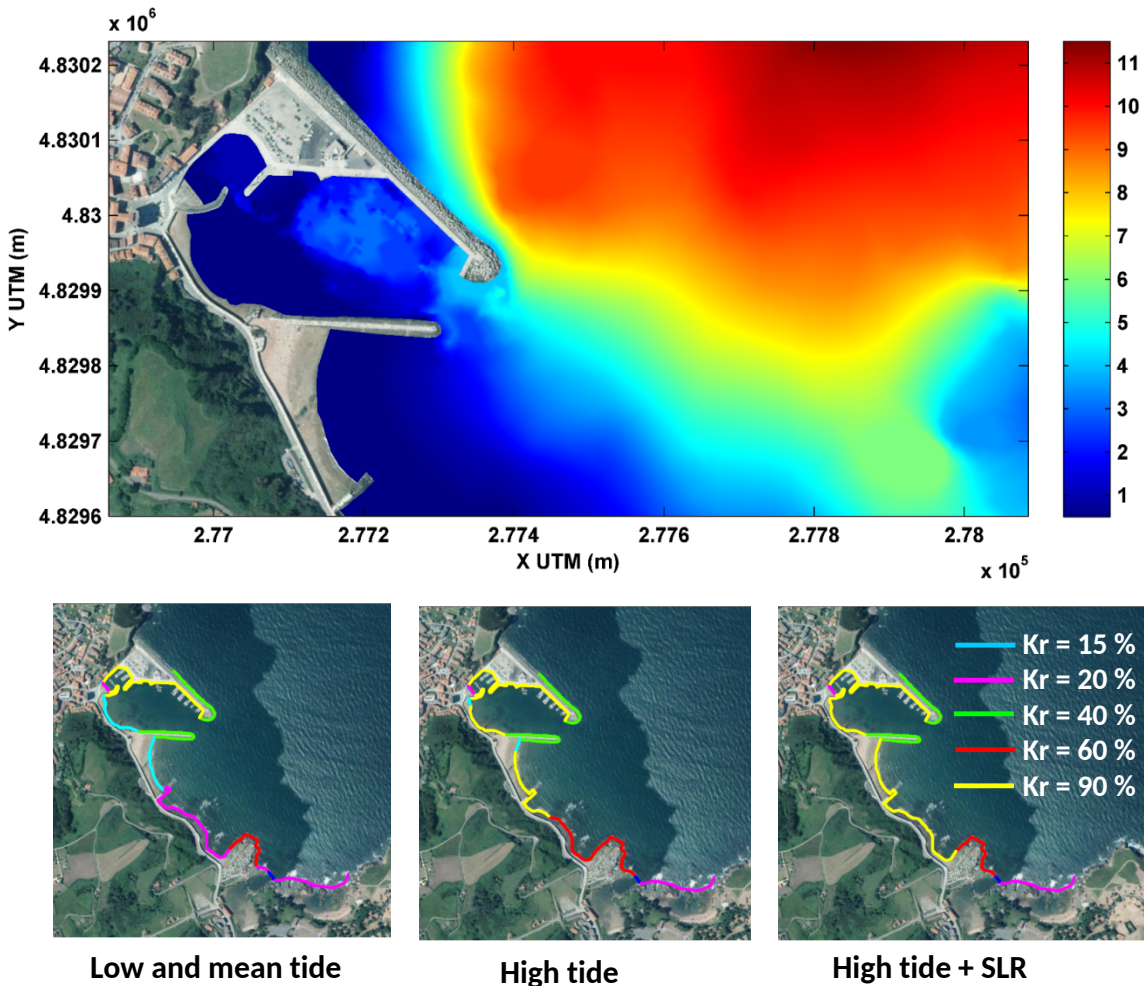
139 The Port of Candás (43° 35, 3' N; 5° 45, 5' W) is located in the region of Asturias (northwest
140 Spain), bordered to the north by the Cantabrian Sea. The current port land area is over 41.150 m²
141 with a berthing length of 72 m. The port's main activities are fishing and recreation (see Figure 1).
142 The water depth in the inner harbor varies between 1 and 3 m (Figure 2). The main breakwater has
143 a trapezoidal cross-section consisting of an outer layer of 23 ton concrete cubes, a secondary layer
144 with 2-3 tons of gravel, a 50-1000 kg rubble layer and a core. A concrete crown wall lies on top
145 of the rubble mound breakwater with a crest level of 11.50 m. The geometry and materials of the
146 different natural and artificial structures of the port's inner boundaries cause changes in wave
147 reflection along these boundaries at different water levels. For this case study these variations were
148 included in the agitation model by using different reflection coefficients along the berths and docks
149 for the four sea levels considered (see Figure 2). Specifically, the following reflection coefficients
150 were considered, according to the typology they represent: dissipative beach ($K_r=0.15$), reflecting
151 beach ($K_r=0.20$), rubble-mound breakwater ($K_r=0.40$), cliff ($K_r=0.60$) and vertical wharf
152 ($K_r=0.9$). For low and mean tide reflection coefficients were kept constant.



153

154 **Figure 1.** Location of the Port of Candás in northern Spain.

155



156

157 **Figure 2.** Upper figure: Bathymetry of the study area (depth in meters). Lower figures: Reflection
 158 coefficients adopted along the port boundaries under different sea levels: low and mean tide, high
 159 tide and high tide + SLR. $K_r=0.15$ for dissipative beach, $K_r=0.20$ for reflecting beach, $K_r=0.40$
 160 for rubble-mound breakwater, $K_r=0.60$ for cliff and $K_r=0.9$ for vertical wharf.

161

162 3 Databases

163 Sea level pressure fields of the Climate Forecast System Reanalysis (CFSR and CFSRv2; [24])
 164 were used to define the predictor of the statistical models explained in section 4. The temporal
 165 coverage spanned from 1979 to 2013, with an hourly temporal resolution and a 0.5° spatial
 166 resolution.

167 The historical wave information used was the high resolution coastal wave database Downscaled
 168 Ocean Waves (DOW, [25]), with a low resolution mesh of $0.01^\circ \times 0.008^\circ$ and several nested meshes
 169 reaching a maximum resolution of 200 m. This database was generated using a hybrid downscaling

170 methodology which combines statistical techniques and dynamical simulations. The Global Ocean
 171 Waves database (GOW, [26]) was used at the regional scale as wave forcing to generate the coastal
 172 wave reanalysis. The SeaWind database, generated by performing a dynamical downscaling of the
 173 NCEP/NCAR wind reanalysis at a spatial scale of 30 km [27], was used as wind forcing. The
 174 results of this hybrid downscaling provided the following hourly sea state parameters from 1948
 175 to 2014: significant wave height (H_s), mean period (T_m), peak period (T_p) and wave direction (θ).

176 The 62-year (1948–2014) high-resolution hindcast of the meteorological sea level component
 177 (storm surge, SS) (GOS 1.1; [28]) was used to determine historical storm surge data. The GOS 1.1
 178 database was developed for Southern Europe using the Regional Ocean Model System (ROMS)
 179 with a horizontal resolution of $1/8^\circ$ (~14 km).

180 The astronomical tide (AT) was reconstructed on an hourly basis at a spatial resolution of 0.25° ,
 181 using harmonic analyses on the outcomes of the global model of ocean tides (TPXO7.2) that
 182 assimilates data from TOPEX/Poseidon missions and tidal gauges for the common period of waves
 183 and storm surge.

184 The regional SLR by 2100 for RCP8.5 scenarios was extracted from global projections of regional
 185 mean sea level values obtained by [29] using a dynamical modeling approach that incorporates
 186 regional contributions of land ice, groundwater depletion and glacial isostatic adjustment,
 187 including gravitational effects due to mass redistribution.

188

189 **4 Methodology and results**

190 The methodology described in Figure 3 is composed of two main parts:

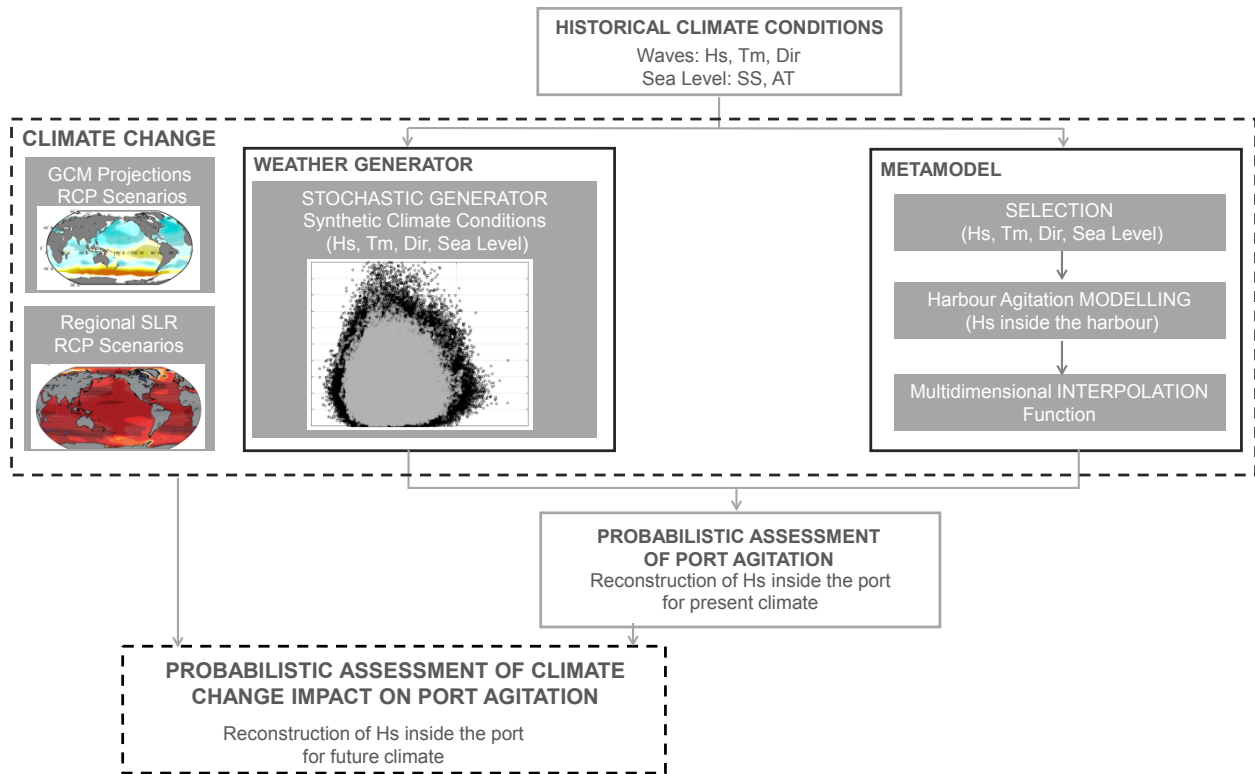
- 191 • A weather generator to derive hourly multivariate marine conditions outside the port.
- 192 • A metamodel to transfer hourly marine conditions outside the port as generated in the
 193 previous step to the inner harbor, in order to obtain wave agitation.

194 The definition of the stochastic generator requires historical information of the forcing conditions
 195 outside the port. The climate emulator based on weather patterns for modelling daily multivariate
 196 events [20] was extended to simulate hourly waves and storm surges at the entrance of the port.
 197 The model is based on a predictor-to-predictand synoptic regression-guided classification [9],
 198 grouping marine conditions according to similar generating meteorological processes, called
 199 weather types (WTs). This method ensures that the predictand within each WT is independent and
 200 identically distributed for the applicability of Gaussian copulas to model the dependence between
 201 variables. Besides, the method captures climate's non-stationary characteristics based on the
 202 variability of WTs over time. A Monte Carlo approximation is applied to stochastically simulate
 203 large samples of hourly conditions at the entrance of the harbor.

204 For the second step, a metamodel based on a hybrid downscaling methodology (a combination of
 205 dynamical and statistical downscaling) developed to generate high resolution nearshore wave
 206 reanalysis databases [25] was adopted. Specifically, a number of representative sea states was
 207 propagated using a model solving the elliptic mild slope (MSP, [30]) and the time series of

208 nearshore wave parameters were reconstructed by means of an interpolation technique. The way
 209 in which the number of simulations was selected from the synthetic data ensured the coverage of
 210 the new multivariate space of climate drivers. The probabilistic assessment of current port
 211 operability due to wave agitation was obtained by reconstructing the significant wave height inside
 212 the port for each simulated hourly condition at the entrance of the harbor for the present climate.

213 To assess climate change impacts on port agitation, climate change can be introduced in the
 214 weather generator by means of future WT probabilities that can be reflected as changes in waves
 215 and storm surges and SLR added to the sea level time series. The metamodel has to be updated to
 216 take into account climate change in those cases selected to be modelled as well as the effect of
 217 SLR on the reflection coefficients to be used in the wave agitation model.

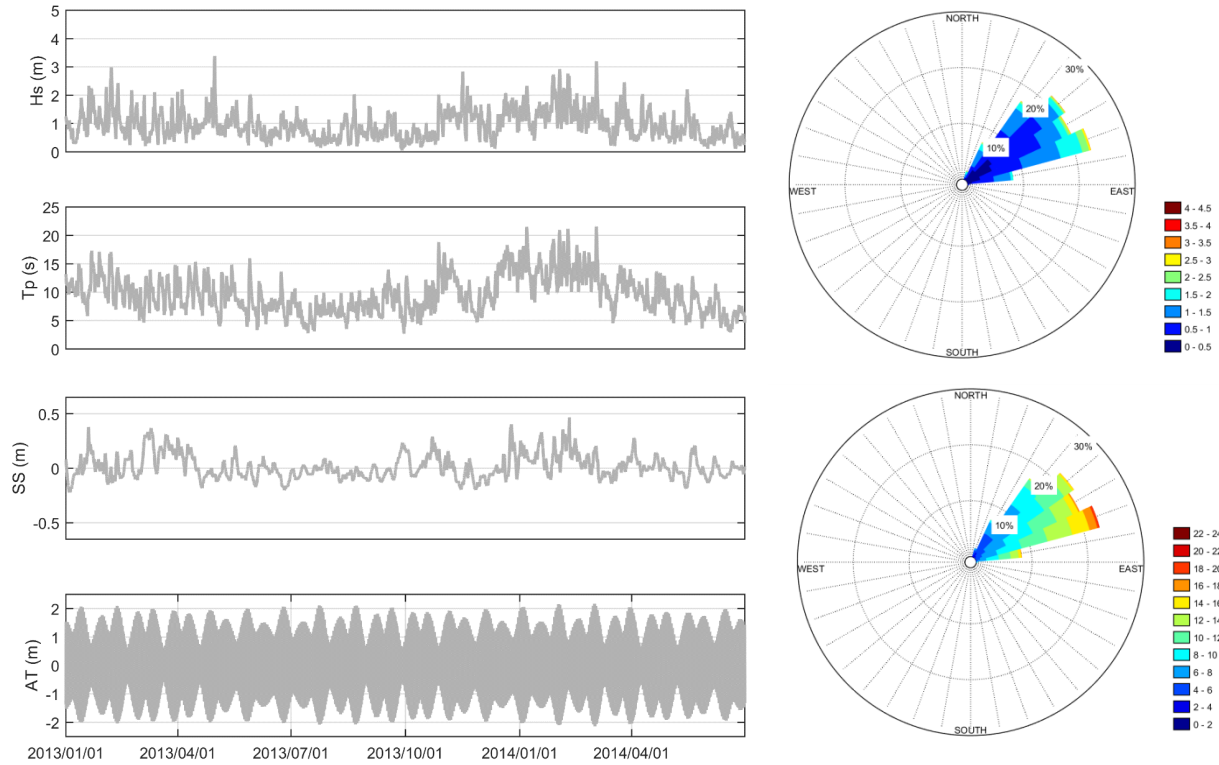


218

219 **Figure 3.** Probabilistic methodology which combines a weather generator and a metamodel to
 220 assess port operability due to wave agitation under present and future conditions.

221

222 Figure 4 shows the time series for years 2013 and 2014 and the distribution of $H_s-\theta$ and $T_p-\theta$ of
 223 the forcing conditions occurring outside the port, obtained from the databases described in section
 224 2. Forcing conditions outside the port were defined at about 6.0 m depth. Wave climate at this
 225 location has suffered an intense refraction due to the protection effect of Cape Peñas (Figure 1)
 226 resulting in wave energy concentration in the N-E sector. The maximum significant wave height
 227 is limited to 4.5 m while peak periods reach values of 20 s which can be combined with storm
 228 surges of almost 0.5 m and high spring tides over 2.0 m.



229

230 **Figure 4.** H_s , T_p , SS and AT values for two years within the time series) at the entrance of the
 231 harbor (left panels). H_s and T_p roses (right panels).

232

233 4.1 Weather generator

234 A weather-type framework was used to model the nonstationary behavior of the local multivariate
 235 predictand (H_s , T_m , T_p , θ and SS) related with large-scale predictors (sea level pressure, SLP). The
 236 daily predictor was classified into a discrete number of weather patterns (WTs) according to their
 237 synoptic similarity. Hourly multivariate events were modelled using a marginal distribution for
 238 each predictand variable and a Gaussian copula within each WT. The stochastic generator follows
 239 similar steps as the one developed by [20] for multivariate extremes, except in this case the
 240 extremal index is not required. The five steps involved in this model are: 1) To collect and pre-
 241 process historical data of the predictor (SLP) and predictands (H_s , T_m , T_p , θ and SS). 2) Define
 242 WTs using a semi-guided classification [31]. 3) Fit a stationary model (e.g. Lognormal,
 243 Generalized Extreme Value) to each variable of the multivariate predictand (H_s , T_m , SS outside the
 244 port) associated with each WT. 4) Model the dependence between predictand variables within each
 245 weather type using a Gaussian copula. 5) Generate synthetic multivariate hourly conditions taking
 246 into account the monthly WT probability and dependence structure associated with each WT.

247 The spatial domain of the predictor should cover the oceanic region responsible for generating
 248 waves arriving at each location of interest. The temporal coverage (recent history) should account
 249 for wave travel time from generation to target location. Based on previous works, the semi-

250 supervised WTs of the grid node from the global collection of WTs at a $1.0^\circ \times 1.0^\circ$ resolution
 251 generated to obtain global wave projections [9] at a location closest to the port of study, was used
 252 to develop the weather generator (steps 1 and 2 in this section). The predictor definition (spatial
 253 domain and temporal coverage) corresponded to the subdomain covering the North Atlantic Ocean
 254 (from an ocean division based on a global wave genesis characterization). The predictor was
 255 defined as the 3-daily mean SLP and 3-daily mean SLPG (squared SLP gradients), calculated daily
 256 throughout the historical time period. More details regarding this characterization and WT
 257 collection can be found in [9]. A regression guided classification was applied to a combination of
 258 the weighted predictor and predictand estimations from a regression model linking the SLP fields
 259 with local marine conditions. The level of influence of the wave and storm surge data was
 260 controlled by a simple weighting factor which balances the loss/gain of predictor/predictand
 261 representativeness. A factor equal to 0.6 was implemented based on previous sensitivity analyses.
 262 A better grouping of the predictand was obtained due to a stronger relation of the WTs with local
 263 marine climate conditions.

264 The long-term marginal distributions (step 3) of hourly H_s , T_m , and SS outside the port within each
 265 WT were fitted to a generalized extreme value (GEV) distribution, a Lognormal distribution or
 266 Unified Distribution Model [32], obtaining the best fit of the central regime with a GEV. The
 267 empirical distribution was used for the wave direction variable. A heteroscedastic model between
 268 T_p and T_m was fitted within each WT. T_p was considered to be normally distributed with parameters
 269 mean and variance being a function of T_m (polynomials with unknown degree). A Gaussian Copula
 270 was used to model the dependence between H_s , T_m , SS and θ (step 4).

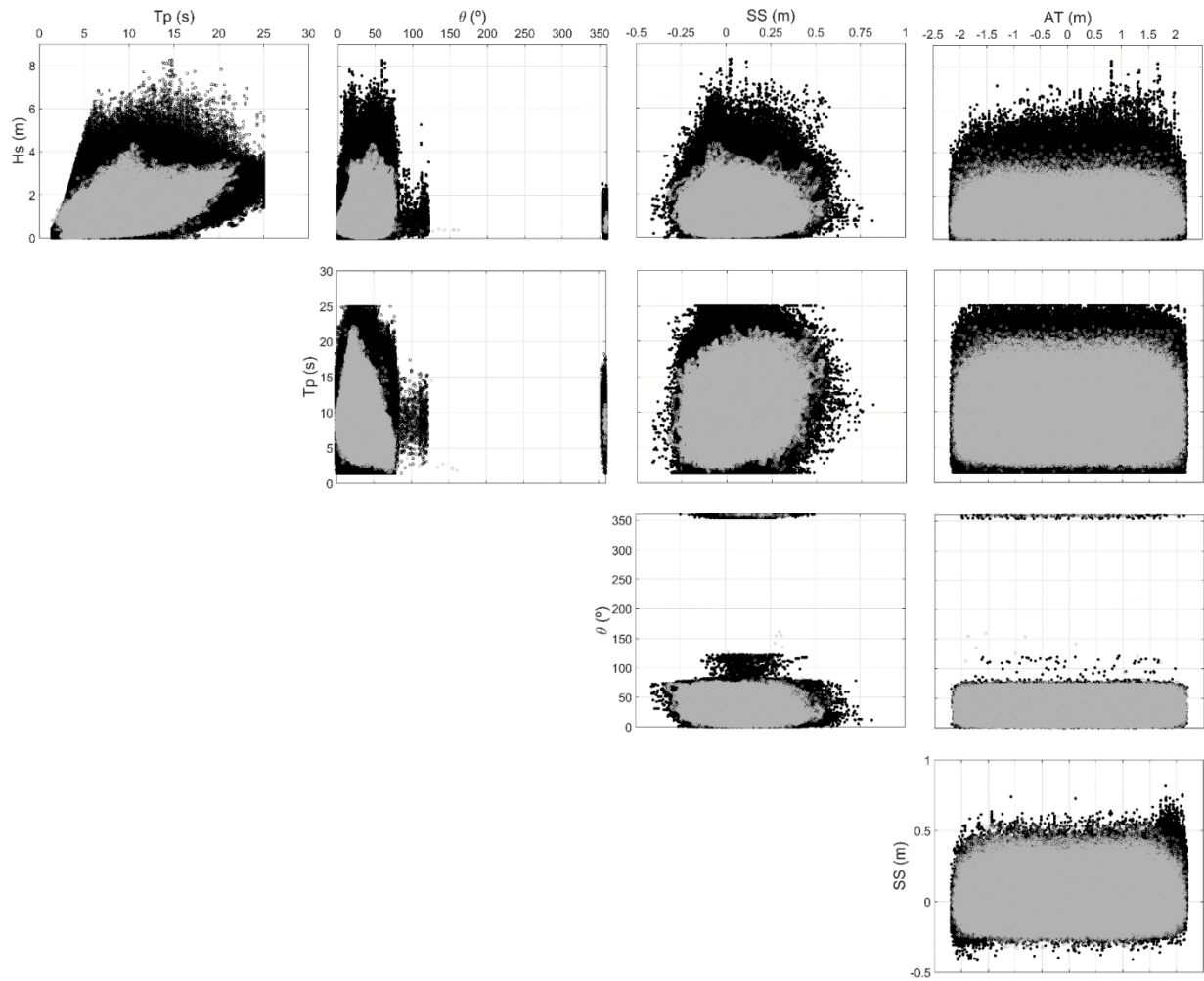
271 The Monte Carlo sampling procedure used to generate synthetic marine conditions (step 5)
 272 requires the following phases: i) Sample a daily WT from a Generalized Bernoulli distribution due
 273 to the categorical choice of one of the $N=100$ WTs. ii) Randomly generate 24 hourly synthetic H_s ,
 274 T_m , θ and SS using the Gaussian copula and the marginal fits associated with the daily simulated
 275 WT; iii) Sample 24 hourly T_p from the heteroscedastic model between T_p and T_m associated with
 276 the daily WT; iv) Independently sample 24 hourly values of astronomical tide from its monthly
 277 empirical distribution. The process is repeated until a synthetic 90-year time series of hourly
 278 multivariate forcing marine conditions is obtained.

279 One thousand, 90-year long, new time series of H_s , T_m , T_p , θ , SS and AT were simulated with the
 280 previously fitted emulator. Each series was generated with a different set of parameters, randomly
 281 taken from the parameter sample obtained considering a Gaussian distribution. Scatter plots of the
 282 five sea-storm variables are shown in Figure 5. The large multivariate sample of hourly forcing
 283 conditions captures the characteristics of dependencies among variables. Wave breaking and wave
 284 steepness limit the maximum simulated wave height. Maximum simulated wave period was
 285 limited to 25 s. The effect of the imposed physical limitations of wave slope can be observed in
 286 the correct reproduction of the relation between wave heights and small wave periods. Figure 6
 287 shows the joint probability density functions of (H_s, T_p) , (H_s, θ) , (H_s, SS) and (T_m, T_p) obtained
 288 from the historical series (blue lines) and from the simulated series (dashed lines). The simulated
 289 series are able to reproduce the main features of the original bivariate distributions. They fail in
 290 representing some details of the distributions, as the clear dependence between wave heights
 291 around 1.0 m and low peak periods.

292

293

294



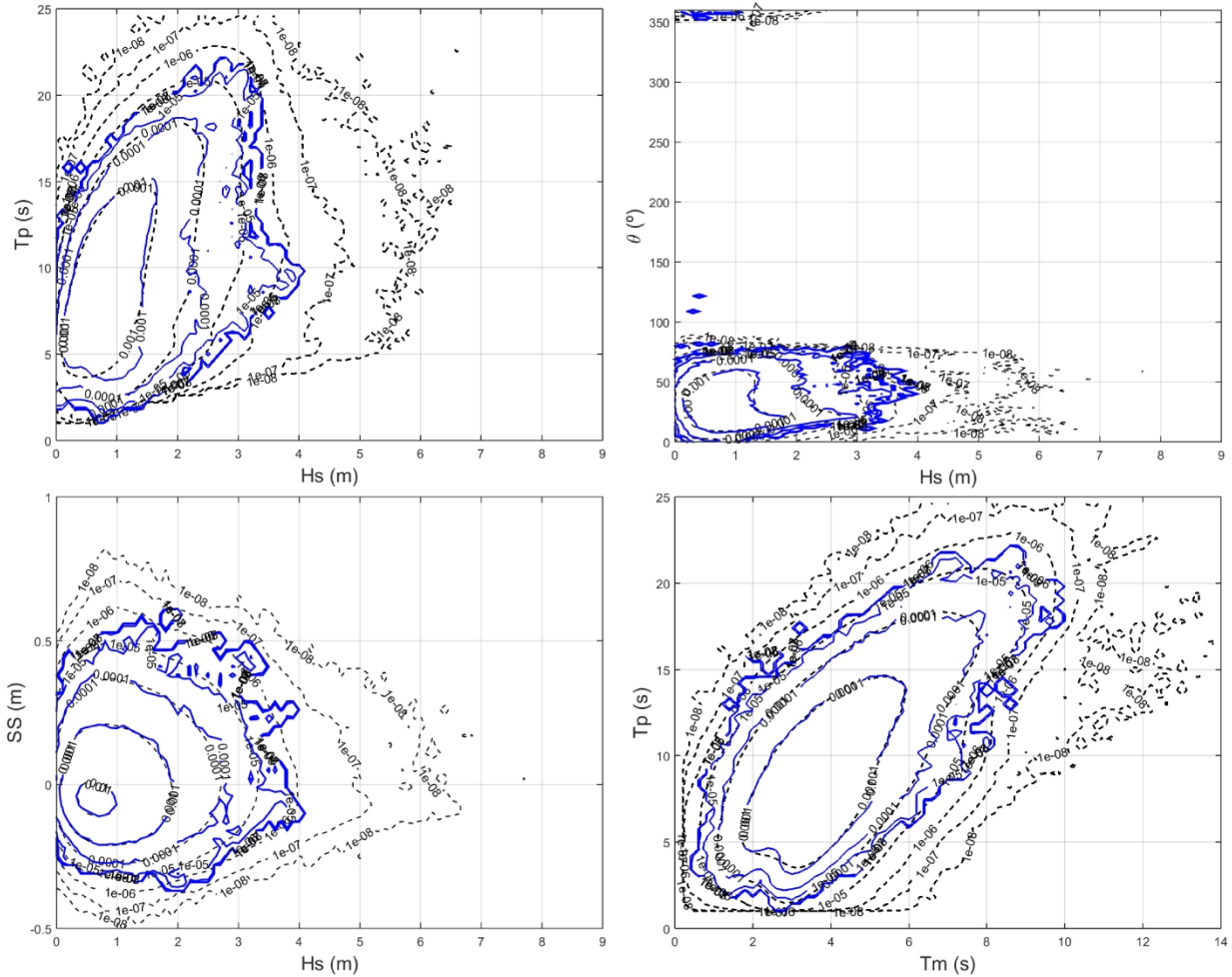
295

296

297 **Figure 5.** Scatter plots of marine climate (H_s , T_p , θ , SS , AT) at the entrance of the port. Historical
 298 data: grey dots; Monte Carlo simulations (1000 samples of 50 years of hourly data): black dots.

299

300

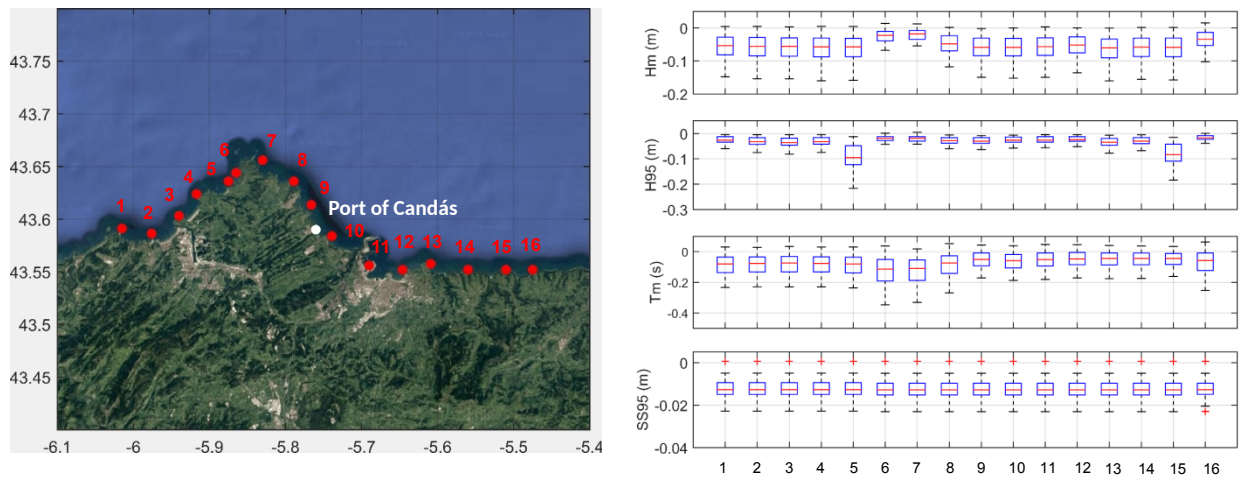


301 ——— Simulations (1000x50 years) ——— Observations (1000x50 years)
 302 **Figure 6.** Joint probability density function of hourly forcing conditions. Blue solid lines represent
 303 the results obtained from the historical data and black dashed lines represent the simulated data
 304 generated using the weather generator.

305

306 Regarding future synthetic time series (e.g. in the period 2010-2100), climate change can be
 307 introduced taking into account changes in storminess by means of future WT probabilities from
 308 GCMs and the increase in the mean sea level. Robust multi-model ensemble projections at high
 309 spatial resolutions ($0.01^\circ \times 0.008^\circ$ using DOW at the reference database) measured over the whole
 310 century (2010–2099) were estimated along the northern coast of Spain [33]. Future wave and storm

311 surge projections were statistically downscaled using a weather-type approach [34] for the same
 312 40 GCMs as in regional wave projections made in Europe [35]. The statistical relationship was
 313 established as in the first steps of the weather generator. In this case, however, the empirical
 314 probability distribution of each sea state parameter (e.g., significant wave height) associated with
 315 each WT was calculated. The distribution of this variable for a certain time period can be estimated
 316 as the sum of the probability of each WT during that period multiplied by the corresponding
 317 empirical distribution. Different statistics (e.g., mean, 95th percentile) can be derived from the
 318 estimated distribution. One of the advantages of this statistical downscaling methodology is that
 319 the scale representativeness of the projections depends on the underlying historical wave databases
 320 used as a reference [9]. Figure 7 shows the multimodel ensemble projections of the annual mean
 321 and the 95th percentile of the significant wave height, the mean period and the 95th percentile of
 322 storm surge in the area surrounding the port for the period 2070–2099 compared with the 1979–
 323 2010 period under the RCP8.5 scenario. Box plots illustrated the uncertainty inherent in future
 324 changes obtained from the 40 GCMs. The outcomes reveal slight decreases in surge and wave
 325 height and period. These changes are assumed to be negligible compared to the effect of SLR in
 326 wave propagation inside the port. Indeed, the decreasing waves and storm surge resulting from
 327 these expected changes would underestimate the need for port operation downtimes.



328

329 **Figure 7.** Regional multimodel projections (RCP8.5, 2070–2099 with respect to 1979–2005) for
 330 the mean and the 95th percentile of wave significant wave height, mean wave period and the 95th
 331 percentile of storm surge along the coastline surrounding the study port.

332

333 Following the approach proposed by [36] to account for the SLR uncertainty in the assessment of
 334 flooding risk, a lognormal distribution was fitted with the mean and standard deviation of the
 335 regional projections produced by [29] for the RCP8.5 scenarios in 2100 (i.e., 0.63 ± 0.20 m at the
 336 study area). The lognormal distribution is considered the most likely distribution representing
 337 future SLR [37], although increased rates of ice sheet loss were not included in this study. The
 338 deciles from fitted lognormal distributions split the SLR data set from each horizon year into ten
 339 equally probable parts, the 2100 deciles being: 0.377 m; 0.454 m; 0.507 m; 0.553 m; 0.599 m;
 340 0.646 m; 0.699 m; 0.763 m; 0.852 m; and 1.025 m, respectively. Ten curves were derived from

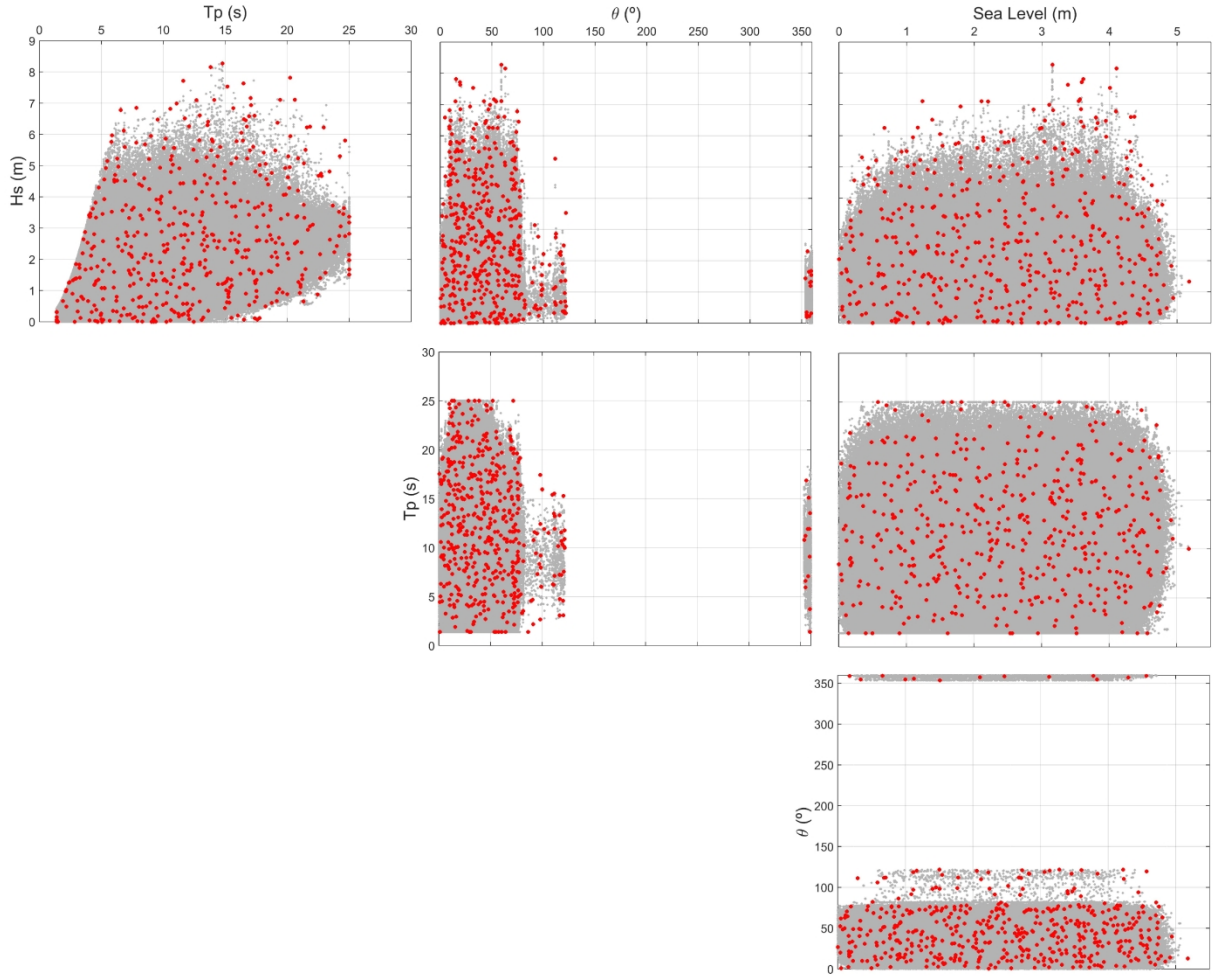
341 local RCP8.5 SLR values in 2025, 2050 and 2100 using a second order polynomial function in
342 order to adopt the shape of those provided by the IPCC [38]. Hourly SLR time series (2010-2100)
343 derived from these curves were added to the synthetic sea level time series (defined as the sum of
344 storm surge and astronomical tide) to define future forcing conditions of port agitation.

345

346 4.2 Metamodel

347 The steps followed to define the metamodel used to transform all the synthetic forcing conditions
348 outside the port were: 1) selection of a limited number of cases comprising the most representative
349 scenarios of wave and sea level fluctuations (storm-surge, astronomical tide and sea level rise)
350 outside the port; 2) a wave agitation strategy to propagate the selected sea states from the entrance
351 of the bay towards the inner harbor zone; 3) reconstruction of the time series of significant wave
352 heights inside the port.

353 A subset of sea states ($M=500$) representative of marine conditions outside the port was selected
354 using the maximum dissimilarity algorithm (MDA, [12]). The MDA identifies a subset comprising
355 the most dissimilar data in a database. The selection starts by initializing the subset through the
356 transference of one vector from the data sample. The remaining elements are selected iteratively,
357 transferring the most dissimilar one from the remaining data in the database to the subset. Figure
358 8 shows the distribution of the selected subset from the MDA over the full multivariate parameter
359 space (H_s , T_p , θ and sea level) covered by the Monte Carlo realizations. The multivariate subset is
360 distributed evenly across the space covering the potential combinations between the four variables
361 with some points selected in the outline of the data space, contributing to an accurate reconstruction
362 of wave agitation conditions inside the port using the proposed metamodel.



363

364 **Figure 8.** Scatter plots of simulated data (grey dots) and the selected cases using the MDA (red
 365 dots in).

366

367 The MSP numerical model [30] was used for wave agitation simulations. This model is able to
 368 solvewave propagation towards and into the harbor, taking into account the refraction, diffraction,
 369 wave breaking and partial reflection imposed by natural and artificial structures (quays, basins,
 370 breakwaters, etc.) and real bathymetry contours. The model provides (2DH) significant wave maps
 371 along the whole numerical domain. A complete spectral sea-state propagation strategy [39] based
 372 on the invocation of a pre-calculated monochromatic wave catalogue was applied to noticeably
 373 reduce the CPU-effort to propagate real wave spectra towards any inner control point. This
 374 technique is based on a three-step method:

375 1. The selection of N monochromatic wave conditions (the combination of periods T and
 376 directions θ) by collapsing the 4D-hypermatrix [frequency, direction, energy, time] for the whole
 377 wave hindcast used, into a single resulting matrix representing the historical energy packs available
 378 in the study zone (for a typical 35 frequency \times 72 direction spectrum matrix, and taking into
 379 account real/theoretical frequency and direction spreading factors for each hour). N can adopt

380 values from 30% to 60% of the total matrix size used, depending on the geographical location of
 381 the harbor/ outer wave climate.

382 2. The numerical propagation of each N monochromatic wave (using a constant wave height
 383 H, because of the linear nature of the model used) and for the different sea levels considered.

384 3. The aggregation of any spectrum by adding all the individual energy packs that define it.

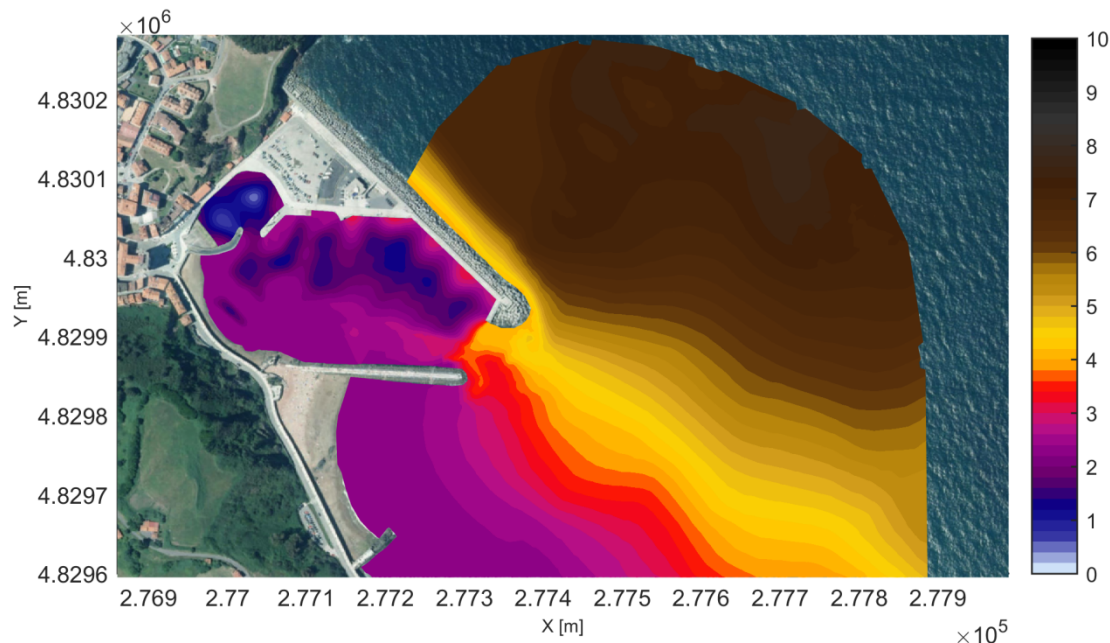
385 For this study additional considerations were established:

386 4. Four water levels were used (total Nx4 monochromatic cases) (three to cover the
 387 astronomical tide range and one as expected upper SLR).

388 5. Changes in reflection coefficients in the model's setup (as described in the study area
 389 section) due to SLR.

390

391 This technique, besides achieving a radical CPU-time reduction, enables to rapidly include any
 392 future scenario needed or sensitivity analysis required, as well as changes in one or many spectrum
 393 variables due to climate change (energy, frequency, direction and its frequency-directional
 394 spreading). On the other hand, this technique could over-predict wave-shoaling effects, especially
 395 for shallow bathymetry zones. Thus, it should be used with caution if non-linear wave-wave
 396 interactions are expected in the study zone, especially for wave breaking related processes and
 397 shoaling. This drawback is minimized for open harbors, with (in general) quasi-constant/ mild
 398 bathymetry configurations within the basins and outer zones, as shown in [39]. Figure 9 shows an
 399 example of a wave agitation map inside the port for conditions outside the port defined by $H_s=7.2$
 400 m; $T_p=15.8$ s; $\theta =54.5^\circ$ and sea level=3.63 m.



401

402 **Figure 9.** Wave agitation map for the following marine conditions outside the port: $H_s=7.2$ m;
403 $T_p=15.8$ s; $\theta =54.5^\circ$ and sea level=3.63 m.

404 The significant wave height time series inside the port are reconstructed using the
405 multidimensional interpolation technique of radial basis functions (RBF, [40]). The RBFs enable
406 a statistical relationship to be defined between the marine parameters characterizing the forcing
407 conditions and the wave height inside the port from the results of the selected cases. The RBF
408 interpolation method defines the function to be approximated by means of a weighted sum of
409 radially symmetric basic functions located at the data points where the results are available. A
410 more detailed description of these statistical tools implemented in the proposed hybrid
411 methodology can be found in [12].

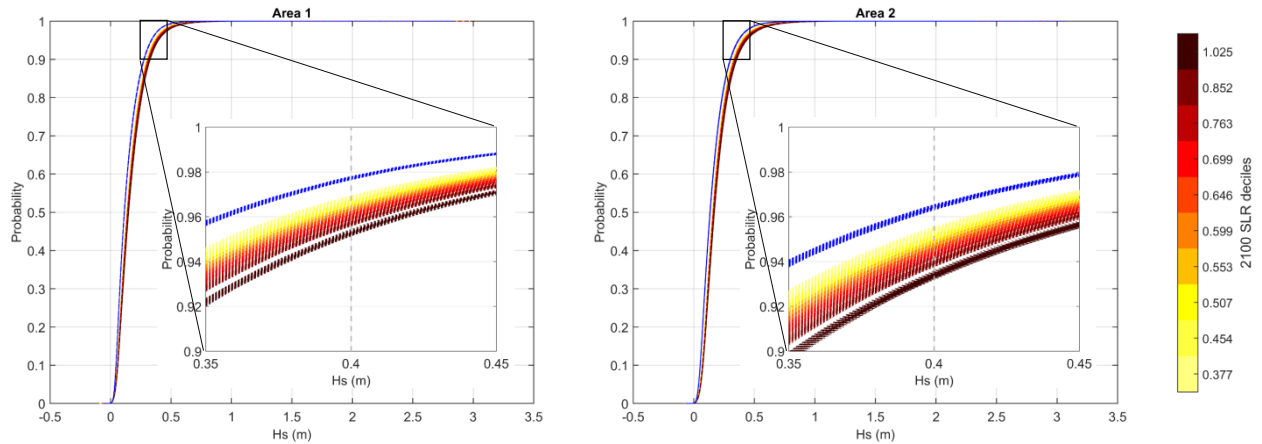
412

413 4.3 Results

414 The synthetic historical time series of marine conditions (waves, storm surge, and astronomical
415 tide) outside the port were transferred inside the port using the corresponding RBF. The synthetic
416 time series outside the port was transformed to the future period 2010-2099 adding the
417 corresponding SLR to each hourly sea level. Their corresponding wave height inside the port was
418 reconstructed applying the RBF.

419 The annual operability or the hours of non-operability are some of the basic port design criteria
420 stipulated by national and/or international standards (such as ROM or PIANC). In this example,
421 hours of non-operability were calculated from each time series as the hours exceeding a certain
422 threshold of H_s inside the port. Here, a threshold of 0.4 m was applied, as suggested in the Spanish
423 Recommendations for Maritime Structures for Fishing Ports (ROM 3.1-99, [41]).

424 Figure 10 shows the historical and future empirical cumulative distributions of significant wave
425 height, H_s , inside the port in Areas 1 and 2 from the one thousand synthetic time series. Fifty-year
426 long time series of forcing conditions were considered in the assessment of the port's downtimes
427 since the useful life of the Port of Candás is established in 50 years. The future distribution was
428 based on the thousand synthetic future hourly time series from 2050-2099 obtained for the ten SLR
429 scenarios sampled from a lognormal distribution of the RCP8.5 SLR projections. The future
430 empirical distributions for the ten SLR scenarios were represented in a yellow-red scale
431 corresponding to the lowest-highest decile, respectively. The probability of a significant wave
432 height lower than 0.4 m (non-operability threshold for fishing ports) is lower the higher the SLR
433 (see the zoomed image of the empirical cumulative distribution between 0.35 to 0.45 m in Figure
434 10).



435

436 **Figure 10.** Historical empirical cumulative distribution (in blue) and future empirical cumulative
 437 distributions for the ten SLR scenarios (in yellow-red scale) of significant wave height inside the
 438 port in Area 1 and Area 2.

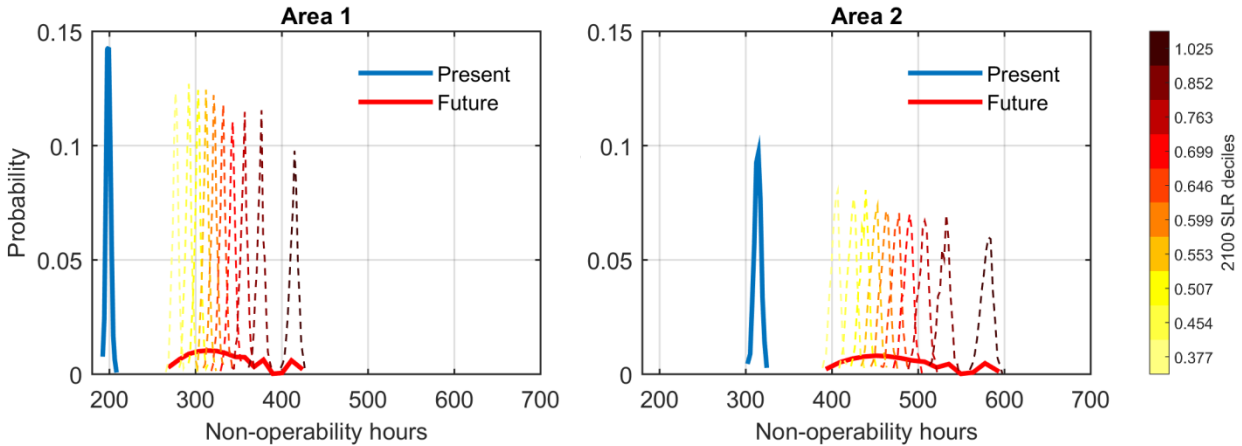
439

440 Hours of non-operability were calculated from the probability (p) obtained for a threshold of 0.4
 441 m as $(1-p) \times 365 \times 24$. The probabilistic distributions of non-operability hours at present (blue) and
 442 future (2050-2099, in red) climate conditions are shown in Figure 11. Future distributions of non-
 443 operability for each RCP8.5 SLR scenario are displayed (dashed lines in the yellow-red color
 444 scale) with the ensemble mean future probabilistic distribution of non-operability (in red). The
 445 ensemble mean distribution was obtained by adding up the distribution for each of the ten SLR
 446 scenarios multiplied by 0.1 (the ten SLR scenarios are sampled with an equal probability). It can
 447 be noted that hours of non-operability do increase from present to future conditions for both areas.

448 The probabilistic distribution of non-operability hours under current climate conditions represents
 449 the uncertainty associated with the historical forcing conditions outside the port. The ensemble
 450 mean future distribution integrates the uncertainty associated with the RCP8.5 SLR scenarios and
 451 the uncertainty due to the forcing conditions outside the port (distributions of non-operability hours
 452 of ten future RCP8.5 SLR scenarios). Besides, higher non-operability hours, as well as a higher
 453 uncertainty, are expected for higher SLR scenarios, as can be observed in wider probabilistic
 454 distributions of non-operability hours the higher the SLR decile (see Figure 11).

455

456



457

458 **Figure 11.** Probabilistic distributions of non-operability hours due to wave agitation in Areas 1
 459 and 2 inside the port in current (in blue) and future (2050-2099) climate conditions in each SLR
 460 scenario (in yellow-red scale) and the future ensemble mean distribution of non-operability hours
 461 (thick red line).

462

463

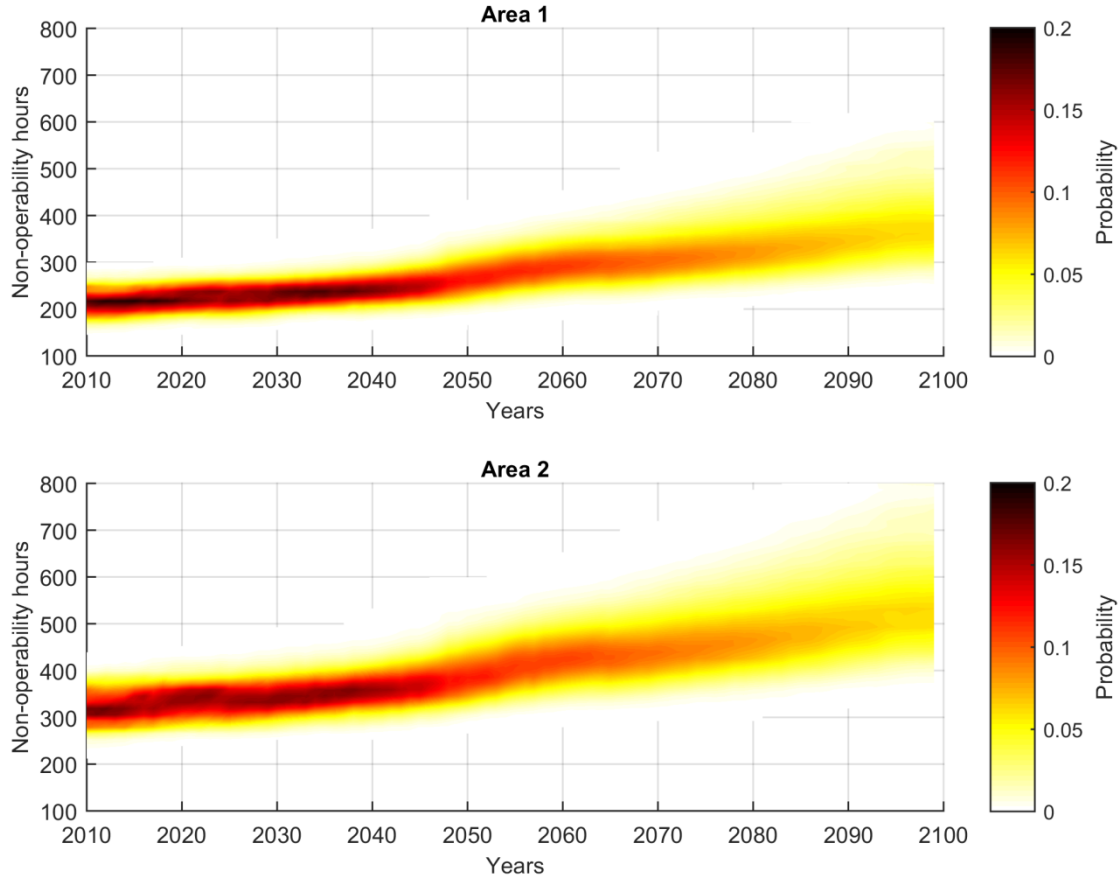
464 One additional way to summarize and compare the results obtained is displayed in Table 1. Each
 465 of the present and future distributions of non-operability hours is fitted to a lognormal distribution.
 466 The mean, standard deviation and coefficient of variation are calculated and shown in the table. In
 467 both Areas 1 and 2, the future mean values for non-operability hours are drastically increased (from
 468 198.90 to 332.13 in Area 1 and from 313.62 to 475.14 in Area 2) due to a mean SLR of 0.257 m
 469 by 2050 and 0.634 m by 2100. The latter increase is due to non-linear interactions between waves
 470 and sea level, and changes in the reflection coefficients associated to SLR. Regarding the
 471 nondimensional coefficient of variation, the uncertainty associated with non-operability hours
 472 increases from about 1.3 % (0.0132 in Area 1 and 0.0129 in Area 2) under current conditions, to
 473 around 10 % (0.1163 in Area 1 and 0.1044 in Area 2) in future ones. These results differ from the
 474 future SLR coefficient of variation (26.7% by 2050 and 31.1% by 2100), indicating that the
 475 magnitude of the SLR uncertainties are reflected to a lower degree in the magnitude of the
 476 uncertainty of non-operability hours.

	RCP8.5 SLR (m)		Non-operability (hours)			
			Area 1		Area 2	
	2050	2100	Present	Future (2050-2100)	Present	Future (2050-2100)
Mean	0.257	0.634	198.90	332.13	313.62	475.14
Std	0.069	0.197	2.625	38.61	4.057	49.604
CV (std/mean)	0.267	0.311	0.0132	0.1163	0.0129	0.1044

477 Table 1: Mean, Standard Deviation and Coefficient of Variation of the lognormal distribution of
478 2050 SLR and 2100 SLR predictions and the lognormal distribution of the non-operability hours
479 for the present and future period in Areas 1 and 2.

480

481 Non-operability hours during the useful life of the infrastructure/port taking into account climate
482 change was calculated along the 21st century adding the evolution of the SLR to the hourly time
483 series of sea level. In the previous analysis of the impact of climate change in the port's operability,
484 future non-operability hours were calculated for a useful life of 50 years, from 2050 to 2100, to
485 obtain more significant changes. However, the assessment of port operability should be adjusted
486 to the projected useful life of the infrastructure, as of its construction. Figure 12 shows the
487 interannual variability of the ensemble's mean probability of non-operability hours from 2010 to
488 2099 in Areas 1 and 2 based on the ten SLR scenarios. First, the empirical distribution of non-
489 operability hours was calculated on a yearly basis for each of the 10 RCP8.5 SLR scenarios
490 considered. Mean sea level rise rates were determined fitting a second order polynomial to the
491 deciles from the local SLR lognormal distribution in 2025, 2050 and 2100. Afterwards, the
492 ensemble mean distribution of non-operability hours was calculated every year. An average
493 moving mean of ten years was applied. A linear trend of the mean hours of non-operability along
494 the 21st century can be observed in Figure 12 (e.g., downtime increases from 320 hours in 2010
495 to 510 hours in 2100). The dispersion of the empirical density distribution rises along the 21st
496 century due to a broader uncertainty of the SLR scenarios as the horizon increases. At the
497 beginning of the 21st century, the SLR distribution spread was limited which is reflected in a
498 narrow ensemble mean distribution of non-operability hours (i.e., high probability centered in the
499 mean value). However, the SLR distribution broadened along the 21st century, increasing the
500 ensemble mean distribution of hours of non-operability (e.g, downtime hours vary from 290 to 400
501 hours in 2010 and from around 400 to 800 in 2100). Changes in non-operability hour values are
502 more significant after 2050 due to a more pronounced acceleration of SLR as of the second half of
503 the 21st century.



504

505 **Figure 12.** Interannual ensemble mean probability of non-operability hours from 2010 to 2099 in
 506 Area 1 and Area2 taking into account the increase in SLR uncertainty along the 21st century.

507

508 **5 Summary and conclusions**

509 A hybrid statistical-dynamical framework was developed with two main purposes: 1) to provide a
 510 probabilistic evaluation of port operability to assess a minimum level of downtime of the port; 2)
 511 to introduce climate change in the assessment of port operability during its useful life.

512 The methodology is strongly dependent on the multivariate nature of climate drivers of wave
 513 agitation such as the combination of waves and sea levels and the availability of these forcings
 514 outside the port. Therefore, the following requirements should be met: 1) the use of a stochastic
 515 generator to model the dependence between multivariate conditions; 2) the application of a
 516 numerical modelling approach to propagate wave offshore conditions inside the port.

517 Hence, the methodology includes: 1) A weather generator based on WTs to take into account future
 518 climate variability through WT probability changes linked to changes in climate drivers (waves
 519 and storm surges); 2) A metamodel based on a catalog of wave propagations and a
 520 multidimensional non-linear interpolation to reconstruct hourly significant wave height time series
 521 inside the port with an accuracy similar to that of the numerical simulations.

522 The case study was focused on port operability due to wave agitation. The methodology allows to
523 transfer thousands of synthetic time series of present and future climate conditions inside the port
524 in order to carry out a probabilistic analysis of port operability. Future changes in non-operability
525 are expressed including both uncertainties associated with marine conditions outside the port and
526 SLR. Climate induced changes in waves and storm surge are considered to be negligible due to
527 the projections obtained in the study area. Uncertainty of forcing conditions outside the port was
528 quantified through the use of a weather generator that allows to generate synthetic time series.
529 SLR uncertainty was introduced equally by sampling its probability distribution in several
530 horizons, while hourly SLR time series were added to the synthetic sea level fluctuations to define
531 the future forcing conditions outside the port. SLR uncertainty was integrated in the future non-
532 operability evaluation joining the contribution of each sampled SLR scenario with its
533 corresponding probability.

534 Obtaining the future distribution of non-operability hours allows calculating the future probability
535 associated with the non-operability exceedance hours threshold established in port design
536 recommendations (i.e. ROM 3.1-99, [41]) during their useful life. The proposed hybrid
537 methodology produces this very useful and relevant outcome to define a specific acceptable
538 operability risk and can be used as a design criterion in new coastal infrastructure or for climate
539 change adaptation plans.

540 Although for this specific pilot case, climate induced changes on waves and storm surges, have
541 been neglected due to their small values, non-linear feedbacks induced by SLR that may produce
542 an amplification of wave conditions in shallow waters [42] have been introduced in the wave
543 agitation model. Future hourly sea conditions are transformed from the harbor's entrance to inside
544 the port considering the non-linearities between tides, surges, waves and SLR. Changes in the
545 reflection coefficient inside the port due to changes in sea level have also been implemented in the
546 wave agitation simulation.

547 The proposed methodology presents several limitations. The synthetic marine conditions are
548 generated without modelling time structure dependence, which would allow performing an
549 analysis of non-operability's persistence. Besides, this version of the climate emulator is not useful
550 for the analysis of extreme conditions. Synthetic extreme events are not time independent and their
551 frequency could be overestimated. Nevertheless, our objective was focused on port operability
552 which should not be conditioned by extreme events.

553 The methodology presented can be extended to further applications such as coastal infrastructure
554 reliability or operability for other functional parameters or marine operations by tailoring the
555 weather generator and selecting the most appropriate numerical model.

556

557 **Acknowledgments**

558 P. C. and C. I. acknowledge the support of the Spanish 'Ministerio de Economía y Competitividad'
559 (MINECO) and the European Regional Development Fund (FEDER) under Grant BIA2015-
560 70644-R (MINECO/FEDER, UE).

561 **References**

- 562 [1] Becker, A., Inoue, S., Fischer, M., Schwegler, B. (2012). Climate change impacts on
563 international seaports: Knowledge, perceptions, and planning efforts among port administrators
564 *Climatic Change*, 110 (1-2), pp. 5-29.
- 565 [2] Chhetri, P., Corcoran, J., Gekara, V., Maddox, C., McEvoy, D. (2014): Seaport resilience to
566 climate change: mapping vulnerability to sea-level rise, *Journal of Spatial Science*, DOI:
567 10.1080/14498596.2014.943311.
- 568 [3] Becker, A.H., Acciaro, M., Asariotis, R., Cabrera, E., Cretegnny, L., Crist, P., Esteban, M.,
569 Mather, A., Messner, S., Naruse, S., Ng, A.K.Y., Rahmstorf, S., Savonis, M., Song, D.-W., Stenek,
570 V., Velegrakis, A.F. (2013). A note on climate change adaptation for seaports: A challenge for
571 global ports, a challenge for global society. *Climatic Change*, 120 (4), pp. 683-695.
- 572 [4] McEvoy, D, Mullett, J, Millin, S, Scott, H & Trundle, A 2013, Understanding future risks to
573 ports in Australia. Work Package 1 of Enhancing the resilience of seaports to a changing climate
574 report series, National Climate Change Adaptation Research Facility, Gold Coast, 77 pp.
- 575 [5] Nicholls, R. J., Hanson, S., Herweijer, C., Patmore, N., Hallegatte, S., Corfee-Morlot, J.,
576 Chateau, J. and Wood, R.M. (2008). Ranking port cities with high exposure and vulnerability to
577 climate extremes: exposure estimates. *Environment Working Papers no.1*, OECD.
- 578 [6] Sánchez-Arcilla, A., Sierra, J.P., Brown, S., Casas-Prat, M., Nicholls, R.J., Lionello, P., Conte,
579 D. (2016). A review of potential physical impacts on harbours in the Mediterranean Sea under
580 climate change. *Regional Environmental Change*, 16 (8), pp. 2471-2484.
- 581 [7] Sierra, J.P., Casas-Prat, M., Virgili, M., Mösso, C., Sánchez-Arcilla, A. (2015). Impacts on
582 wave-driven harbour agitation due to climate change in Catalan ports. *Natural Hazards and Earth
583 System Sciences*, 15 (8), pp. 1695-1709.
- 584 [8] Sierra, J.P., Genius, A., Lionello, P., Mestres, M., Mösso, C., Marzo, L. (2017). Modelling the
585 impact of climate change on harbour operability: The Barcelona port case study. *Ocean
586 Engineering*, 141, pp. 64-78.
- 587 [9] Camus, P., Losada, I.J., Izaguirre, C., Espejo, A., Menéndez, M., Pérez, J. (2017). Statistical
588 wave climate projections for coastal impact assessments. *Earth's Future*, 5 (9), pp. 918-933.
- 589 [10] Ranasinghe, R., 2016. Assessing climate change impacts on open sandy coasts: a review.
590 *Earth-Sci. Rev.* 160, 320–332.
- 591 [11] Gouldby, B., Méndez, F.J., Guanche, Y., Rueda, A., Mínguez, R., 2014. A methodology for
592 deriving extreme nearshore sea conditions for structural design and flood risk analysis. *Coastal
593 Eng.* 88, 15–26.
- 594 [12] Camus, P., F. J. Mendez, R. Medina (2011). A hybrid efficient method to downscale wave
595 climate to coastal areas. *Coastal Engineering*, 58 (9), 851-862.
- 596 [13] Gouldby, B., Wyncoll, D., Panzeri, M., Franklin, M., Hunt, T., Hames, D., Tozer, N., Hawkes,
597 P., Dornbusch, U., Pullen, T. (2017). Multivariate extreme value modelling of sea conditions
598 around the coast of England. *Proceedings of the Institution of Civil Engineers: Maritime
599 Engineering*, 170 (1), pp. 3-20.

- 600 [14] López, I., López, M., Iglesias, G. (2015). Artificial neural networks applied to port operability
601 assessment. *Ocean Eng.* 109, 298–308.
- 602 [15] ROM 0.0 (2001) General Procedure & Requirements for Design of Maritime & Harbour
603 Structures (Part I); Puertos del Estado. www.puertos.es ISBN 84-88975-31-7
- 604 [16] Heffernan, J.E., Tawn, J.A., 2004. A conditional approach for multivariate extreme values
605 (with discussion). *J. R. Statist. Soc.* 66 (3), 497–546.
- 606 [17] Wahl, T., C. Mudersbach, and J. Jensen (2012), Assessing the hydrodynamic boundary
607 conditions for risk analyses in coastal areas: A multivariate statistical approach based on Copula
608 functions, *Nat. Hazards Earth Syst. Sci.*, 12(2), 495–510.
- 609 [18] Corbella, S., and D. D. Stretch (2013), Simulating a multivariate sea storm using Archimedean
610 copulas, *Coastal Eng.*, 76, 68–78.
- 611 [19] Wahl, T., Plant, N.G., Long, J.W., 2016. Probabilistic assessment of erosion and flooding risk
612 in the northern Gulf of Mexico. *J. Geophys. Res. Oceans* 121. doi: 10.1002/2015JC011482.
- 613 [20] Rueda, A., Camus, P., Tomás, A., Vitousek, S., Méndez, F.J. (2016). A multivariate extreme
614 wave and storm surge climate emulator based on weather patterns. *Ocean Modelling*, 104, 242-
615 251.
- 616 [21] Guedes Soares, C. and C. Cunha (2000). Bivariate autoregressive models for the time series
617 of significant wave height and mean period. *Coastal Engineering* 40, 297–311.
- 618 [22] Solari, S., van Gelder, P.H., (2012). On the use of vector autoregressive VAR and regime
619 switching VAR models for the simulation of sea and wind state parameters. In: Carlos Guedes
620 Soares, et al. (Eds.), *Marine Technology and Engineering*. Taylor & Francis Group, London,
621 pp.217–230.
- 622 [23] Solari, S., Losada, M.T. (2016). Simulation of non-stationary wind speed and direction time
623 series. *Journal of Wind Engineering and Industrial Aerodynamics*, 149, pp. 48-58.
- 624 [24] Saha, S., S. Moorthi, X. Wu, J. Wang, S. Nadiga, P. Tripp, D. Behringer, Y.T. Hou, H.Y.
625 Chuang, M. Iredell, M. Ek, J. Meng, R. Yang, M.P.n. Mendez, H. van den Dool, Q. Zhang, Wang,
626 M. Chen and E. Becker (2014), The NCEP Climate Forecast System Version 2. *Journal of Climate*
627 27, 2185-2208, doi: 10.1175/JCLI-D-12-00823.1.
- 628 [25] Camus, P., Méndez, F.J., Medina, R., Tomás, A., Izaguirre, C. (2013). High resolution
629 downscaled ocean waves (DOW) reanalysis in coastal areas. *Coastal Engineering*, 72, 56-68.
- 630 [26] Reguero, B.G., Menéndez, M., Méndez, F.J., Mínguez, R., Losada, I.J. (2012). A Global
631 Ocean Wave (GOW) calibrated reanalysis from 1948 onwards *Coastal Engineering*, 65, pp. 38-
632 55.
- 633 [27] Menendez M, García-Díez M, Fita L, Fernández J, Méndez FJ, Gutiérrez JM (2013) High-
634 resolution sea wind hindcasts over the Mediterranean area. *Clim Dyn.* doi:10.1007/s00382-013-
635 1912-8
- 636 [28] Cid A, Castanedo S, Abascal AJ, Menéndez M, Medina R (2014) A high resolution hindcast
637 of the meteorological sea level component for Southern Europe: the GOS dataset. *Clim Dyn.*
638 doi:10.1007/s00382-013-2041-0.

- 639 [29] Slangen, A.B.A., M. Carson and C.A. Katsman (2014), Modelling twenty-first century
640 regional sea-level changes, *Clim Change*, doi:10.1007/s10584-014-1080-9.
- 641 [30] GIOC, 2000. MSP: A Finite element model for wave agitation in ports. Technical Report and
642 User Manual. Universidad de Cantabria (in Spanish).
- 643 [31] Cannon, A. J. (2012), Regression-guided clustering: A semisupervised method for circulation-
644 to-environment synoptic classification, *J.Appl.Meteorol. Climatol.*, 51, 185–190.
645 <https://doi.org/10.1175/jamc-d-11-0155.1>.
- 646 [32] Solari, S., Losada, M.A. (2012b). Unified distribution models for met-ocean variables:
647 Application to series of significant wave height. *Coastal Engineering*, 68, pp. 67-77.
- 648 [33] Toimil, A., Losada, I.J., Camus, P., Díaz-Simal, P. (2017). Managing coastal erosion under
649 climate change at the regional scale. *Coastal Engineering*, 128, pp. 106-122.
- 650 [34] Camus, P., Menéndez, M., Méndez, F.J., Izaguirre, C., Espejo, A., Cánovas, V., Pérez, J.,
651 Rueda, A., Losada, I.J., Medina, R., 2014. A weather-type statistical downscaling framework for
652 ocean wave climate. *Journal of Geophysical Research*, DOI: 10.1002/2014JC010141
- 653 [35] Perez, J., Menendez, M., Camus, P., Mendez, F.J., Losada, I.J. (2015). Statistical multi-model
654 climate projections of surface ocean waves in Europe. *Ocean Modelling*, 96, 161-170.
- 655 [36] Quinn, N., P. D. Bates, and M. Siddall (2013). The contribution to future flood risk in the
656 Severn Estuary from extreme sea level rise due to ice sheet mass loss, *J. Geophys. Res. Oceans*,
657 118, 5887–5898, doi:10.1002/jgrc.20412.
- 658 [37] Bamber, J. L., and W. P. Aspinall (2013), An expert judgement assessment of future sea level
659 rise from the ice sheets, *Nat. Clim. Change*, 3, 424–427, doi:10.1038/nclimate1778.
- 660 [38] IPCC 2013. Climate Change 2013: The Physical Science Basis. Contribution of Working
661 Group I to the Fifth Assessment Report of the Intergovernmental Panel on Climate Change
662 [Stocker, T.F., D. Qin, G.-K. Plattner, M. Tignor, S.K. Allen, J. Boschung, A. Nauels, Y. Xia, V.
663 Bex and P.M. Midgley (eds.)].
- 664 [39] Diaz-Hernandez, G., Mendez, F.J., Losada, I.J., Camus, P., Medina, R. (2015). A nearshore
665 long-term infragravity wave analysis for open harbours. *Coastal Engineering*, 97, 78-90.
- 666 [40] Rippa, S., 1999. An algorithm for selecting a good value for the parameter c in radial basis
667 function interpolation. *Advances in Computational and Mathematical* 11, 193–210
- 668 [41] ROM 3.1 (1999) Maritime Port Configuration Design: Approach channel & Harbour basin;
669 Puertos del Estado www.puertos.es ISBN 84-88975-52-X
- 670 [42] Arns, A., S. Dangendorf, J. Jensen, S. Talke, J. Bender, and C. Pattiaratchi (2017). Sea-level
671 rise induced amplification of coastal protection design heights, *Sci. Rep.*, 7, art. no. 40171.
672 <https://doi.org/10.1038/srep40171>.

673

1 Probabilistic Assessment of Port Operation Downtimes Under Climate Change

2
3 P. Camus, A. Tomás, G. Díaz-Hernández, B. Rodríguez, C. Izaguirre, I. J. Losada

4 Affiliation for all authors. *Environmental Hydraulics Institute, Universidad de Cantabria - Avda.*
5 *Isabel Torres, 15, Parque Científico y Tecnológico de Cantabria, 39011, Santander,*
6 *Spain*~~Environmental Hydraulics Institute “IH Cantabria”, Universidad de Cantabria, Spain~~

7
8
9 Corresponding author: Paula Camus (camusp@unican.es)

14 Abstract

15 Disruptions in harbor operations have significant implications for ~~the~~ local, regional and global
16 economies due to ports' strategic role as part of the supply chain. A probabilistic evaluation of
17 port operations ~~taking into account~~ considering the influence of climate change ~~is~~ required in order
18 to secure optimal exploitation during their ports' useful life. Here, we propose a hybrid statistical-
19 dynamical framework ~~is proposed~~ combining a weather generator and a metamodel. The stochastic
20 generator is based on weather types to project climate variability on to hourly multivariate
21 dependent climate drivers outside ~~the~~ ports. The metamodel efficiently transforms hourly sea
22 conditions from the entrance of the harbor towards the inside ~~the~~ port adding leveraging the
23 advantages of a physical process model. Thousands of hourly synthetic time series based on at
24 present climate conditions and ~~in the~~ future ones were transferred inside the port to perform a
25 probabilistic analysis of port operations. Future forcing conditions were defined adding several
26 sea level rise (SLR) scenarios, sampled from their probability distribution, to the synthetic sea
27 level fluctuations time series. Wave amplification due to non-linear interactions between waves
28 and sea level variations and changes in the reflection coefficients inside the port induced by SLR
29 were modelled. Probabilistic future changes of operation downtimes were quantified
30 considering with the uncertainty associated with the historical forcing conditions outside the port
31 and ~~the~~ likely SLR sea level rise scenarios. The ~~application of the~~ methodology was applied to a
32 specific a case study on of a regional port located ~~in~~ the north coast of Spain, were ~~is described~~
33 ~~for~~ port operability due to wave agitation was assessed.

40

41 **1 Introduction**

42 Port ~~infrastructures~~ ~~is~~ ~~are~~ are strategic ~~infrastructures~~ ~~for~~ ~~for~~ local, regional and global economic
 43 growth and development. They play a crucial role as transportation hubs and gateways for the vast
 44 ~~of~~ majority of goods transported around the world, linking local and national supply chains to
 45 global markets. Moreover, demands on ports are likely to grow ~~in the light of expected increases~~
 46 ~~in world freight volumes~~, due to ~~shipping~~ ~~shipping's~~ ~~efficiencies~~ ~~efficiency~~ of shipping and its
 47 smaller carbon footprint ~~compared~~ ~~relative~~ to other modes of transport ~~when dealing with an~~
 48 ~~expected increase in world freight volumes~~ [1]. Other economic activities, including industry,
 49 tourism and fisheries, also flourish around seaports. ~~Thus,~~ ~~A~~any significant disruption in the
 50 logistics of seaports can have significant ~~economic~~ implications ~~for the economy~~ [2]. Service
 51 disruptions alone can cause ~~considerable~~ ~~total~~ economic losses in the order of billions of dollars
 52 and may have important second-order consequences, not only for ~~the~~ regional economies and the
 53 quality of life of those who depend ~~directly~~ on the port's functionality, but also for the operation
 54 of global supply-chains [3].

55 ~~Due to the type~~ ~~By the nature~~ of ~~their~~ businesses ~~held around them~~, seaports are located in one of
 56 the most vulnerable areas to climate change impacts, ~~i.e.:~~ ~~in~~ coastal areas susceptible to sea level
 57 rise and increased storm intensity and/or ~~at~~ mouths of rivers susceptible to flooding [1]. ~~The~~
 58 ~~a~~ ~~Despite this,~~ attention to climate-related impacts in ports is relatively recent [4]. The first
 59 ~~international~~ benchmark studies ~~consisted of~~ ~~are at international scale:~~ an analysis of the most
 60 vulnerable ~~to climate change~~ port cities ~~to climate change~~ in 2070 [5] based on ~~population and~~
 61 ~~asset~~ exposure ~~of population and assets to a~~ water levels defined as one hundred year storm surge,
 62 ~~and~~ a worldwide survey ~~sent to~~ ~~of~~ Port Authorities to detect sectorial ~~'s~~ risk perceptions
 63 ~~regarding about port risks due to~~ climate change ~~on ports~~ [1], ~~respectively~~.

64 The ~~first main first~~ step in the evaluation of climate change impacts ~~on ports~~ involves reviewing
 65 ~~all the~~ potential impacts ~~of climate change on ports,~~ and identifying the main marine variables and
 66 the ~~available~~ databases ~~available where this information is included~~ ~~to obtain and process the~~
 67 ~~relevant information~~ [6]. Sea-level rise used to be the only climate-driver ~~to be~~ considered in the
 68 assessment of climate change impacts, as for example, in the methodology proposed to map
 69 vulnerability of port assets to sea-level rise relative to their location [2]. Future wave and storm
 70 surge conditions are not available from Global Circulation Models (GCMs) for different
 71 Representative Concentration Pathways (RCPs) scenarios which are the primary tools for
 72 investigating the evolution of the climate system over this century. ~~Therefore,~~ ~~A~~a downscaling
 73 approach is required to obtain ~~such~~ future projections ~~of waves and storm surge~~ in order to ~~take~~
 74 ~~them into account when assessing~~ ~~introduce these changes in the assessment of~~ the impact of
 75 climate change in ports. The assessment of climate change effects on port operability (wave
 76 agitation) has been already explored considering changes in waves using various Regional
 77 Circulation Models (RCMs) for an A1B scenario [7], or by adding the effect of ~~sea level rise (SLR)~~
 78 in combination ~~with~~ wave changes for one GCM for RCP8.5 [8]. Another example is the
 79 simplified approach presented in [9] to assess, ~~at regional scale,~~ impacts ~~on port operation~~ due to
 80 overtopping ~~at the regional scale~~ ~~on port operation~~. This approach consists of a direct statistical
 81 weather-typing downscaling of impact indicators (e.g., number of hours per year with overtopping
 82 exceeding a certain threshold), integrating changes in storminess including waves, storm surge and
 83 sea level rise. One of the ~~a~~ advantages of this statistical downscaling method is that it allows ~~to~~

84 quantify the uncertainty associated to coming from different scenarios and climate models (30
 85 GCMs for 2 RCPs were projected), which is not possible if only one or a limited number of
 86 GCMs or RCMs are considered.

87 Climate drivers for evaluating infrastructure reliability or port operability are defined outside the
 88 port, before local nearshore processes such as breaking, diffraction, or reflection have taken place.
 89 Each hourly set of multivariate marine conditions at the entrance of the harbor has to be propagated
 90 inside the port using a wave model at high spatial resolution. When in the case of assessing climate
 91 change is assessed to provide useful information for developing effective adaptation strategies,
 92 thousands of different combinations of future forcing variables must be simulated to account for
 93 the cascading uncertainty associated with the various scenarios and global/regional models [10].
 94 This multi-scale modelling approach is unaffordable computationally. However, a wide variety
 95 of metamodels have been proposed to run wave models for large data sets within a reasonable
 96 computational time. Metamodels are, in essence, simplified (and hence computationally efficient)
 97 representations of computationally intensive models [11]. The traditional approach is to
 98 develop a 'look-up table' which involves running the model for a subset of events defined over
 99 a regular grid with a coarse resolution to limit the number of simulations. Two approaches with a
 100 different degree of complexity can be applied to predict the results for additional events: selecting
 101 the result of the most similar design point as representative of the new event [8], or by using linear
 102 interpolation techniques. More sophisticated methods are developed based on the combination of
 103 a selection algorithm and radial basis functions [12]. This method has been proved to be quite
 104 efficient [13] since it represents the selected input boundary conditions properly and proposes a
 105 due to the proper representation of the selected input boundary conditions and the powerful
 106 interpolation technique. Another alternative which doesn't involve without numerical
 107 simulations consists of applying artificial neural networks to assess port operability [14], but they
 108 require instrumental data outside and inside the port.

109 Furthermore, to assess the safety, serviceability and exploitation of port operations, the Spanish
 110 Recommendations for Maritime Structures (ROM 0.0-0.1, [15]) proposes a Level III Verification
 111 Method based on Monte Carlo methods, for the probabilistic evaluation of failure modes and
 112 operational stoppage modes (downtime) of maritime structures. Modes of failure or operability are
 113 determined by non-linear interactions of multiple meteo-oceanic dynamics (e.g., astronomical tide,
 114 storm surge, waves), being climate drivers (waves and storm surge) being statistically dependent
 115 due to a common synoptic-scale atmospheric circulation generation. It is therefore necessary to
 116 use simulation methodologies that address the dependency between/among variables. There is a
 117 wide range of multivariate statistical models that have been applied to marine conditions.
 118 Depending on the type of outputs they provide, models can be divided into two categories: 1)
 119 extreme events such as unconditional approaches ([16], [11]); copula methods ([17], [18], [19]);
 120 weather-type based models [20] and 2) time series using autoregressive models ([21], [22], [23]).
 121 The use of a Monte-Carlo methods for probabilistic analysis demands a high computational effort
 122 to assess infrastructure failure modes or port operability. The process is even more complex if the
 123 probabilistic verification is also performed including climate change projections.

124 To our knowledge, only one study has evaluated the effect of climate change in port operability
 125 caused by wave agitation due to SLR (three values) and wave changes from one GCM. A
 126 metamodel based on the 40 simulations of wave propagation inside the port is/was? applied [8].
 127 The inoperability time was is obtained as the sum of the frequencies of occurrence from the wave
 128 sets exceeding a fixed threshold. No Any assessment of port operation downtimes due to wave

129 agitation has been performed using a Monte-Carlo approach, ~~nor moreover~~ including climate
130 change.

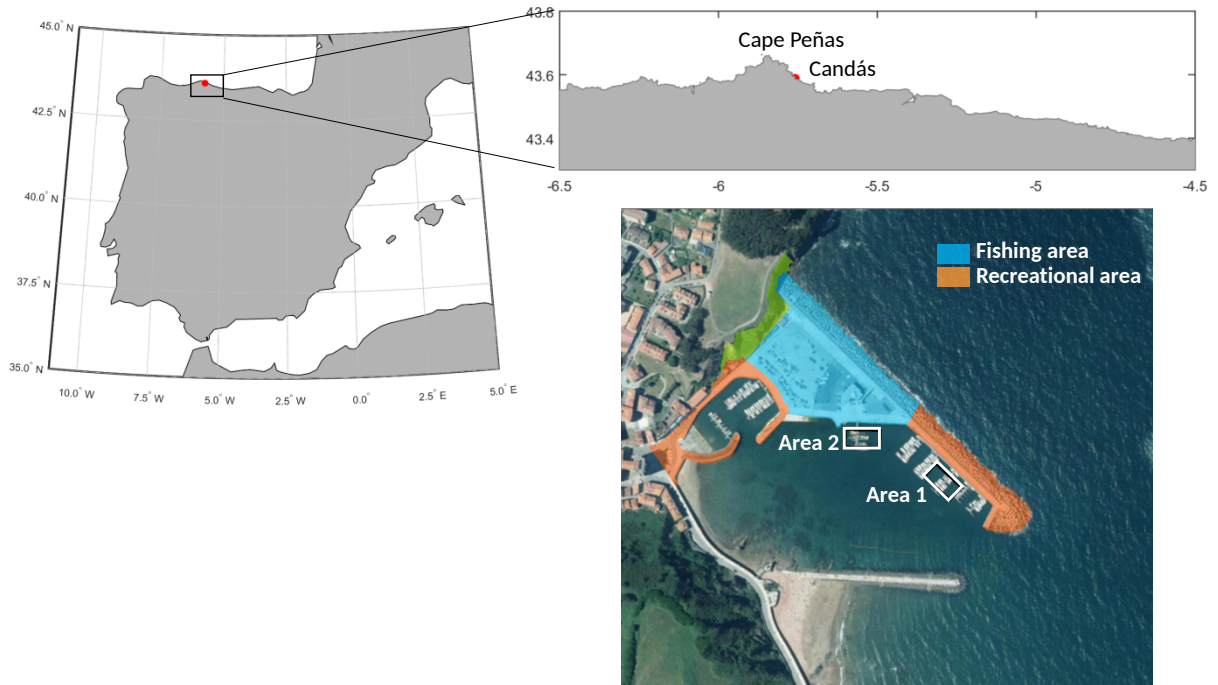
131 In this work, ~~we propose~~ an integrated methodology for very long-term probabilistic assessments ~~at~~
132 of port operability due to wave agitation, including the potential effects of climate change ~~is~~
133 ~~proposed~~. Only port operability due to wave agitation ~~was~~ considered in order to simplify the
134 ~~methodology's~~ description, ~~of the methodology~~ but ~~the method it~~ can be easily extended/~~used~~
135 ~~for to~~ other applications. The probabilistic verification comprises the use of: 1) a stochastic
136 generator which simulates synthetic multivariate forcing conditions at the entrance of the harbor;
137 and 2) a metamodel to transfer these marine conditions inside the port. Synthetic hourly conditions
138 of wave agitation ~~under at~~ present and future climate ~~conditionss wereare~~ evaluated to obtain a
139 probabilistic characterization of port operability and to assess changes due to climate change.
140 Probabilistic sea level rise (SLR) scenarios ~~wereare~~ considered to account for SLR uncertainty in
141 the evaluation of future operation downtimes. The application of the methodology ~~was~~
142 particularized to a regional fishing port currently experiencing recurrent downtimes.

143 The paper is organized as follows: section 2 describes the study area used as a pilot case; section
144 3 presents the databases required for the application of the methodology and section 4 provides
145 extensive details on the overall methodology which combines a weather generator and a
146 metamodel and describes the impact of climate change on port operations. The application ~~of the~~
147 ~~methodology~~ to the regional port is presented throughout sections 2–4 ~~in order to facilitate its~~
148 ~~understanding the understanding of the methodology~~. Finally, section 5 summarizes and concludes
149 the work.

150

151 2 Study area

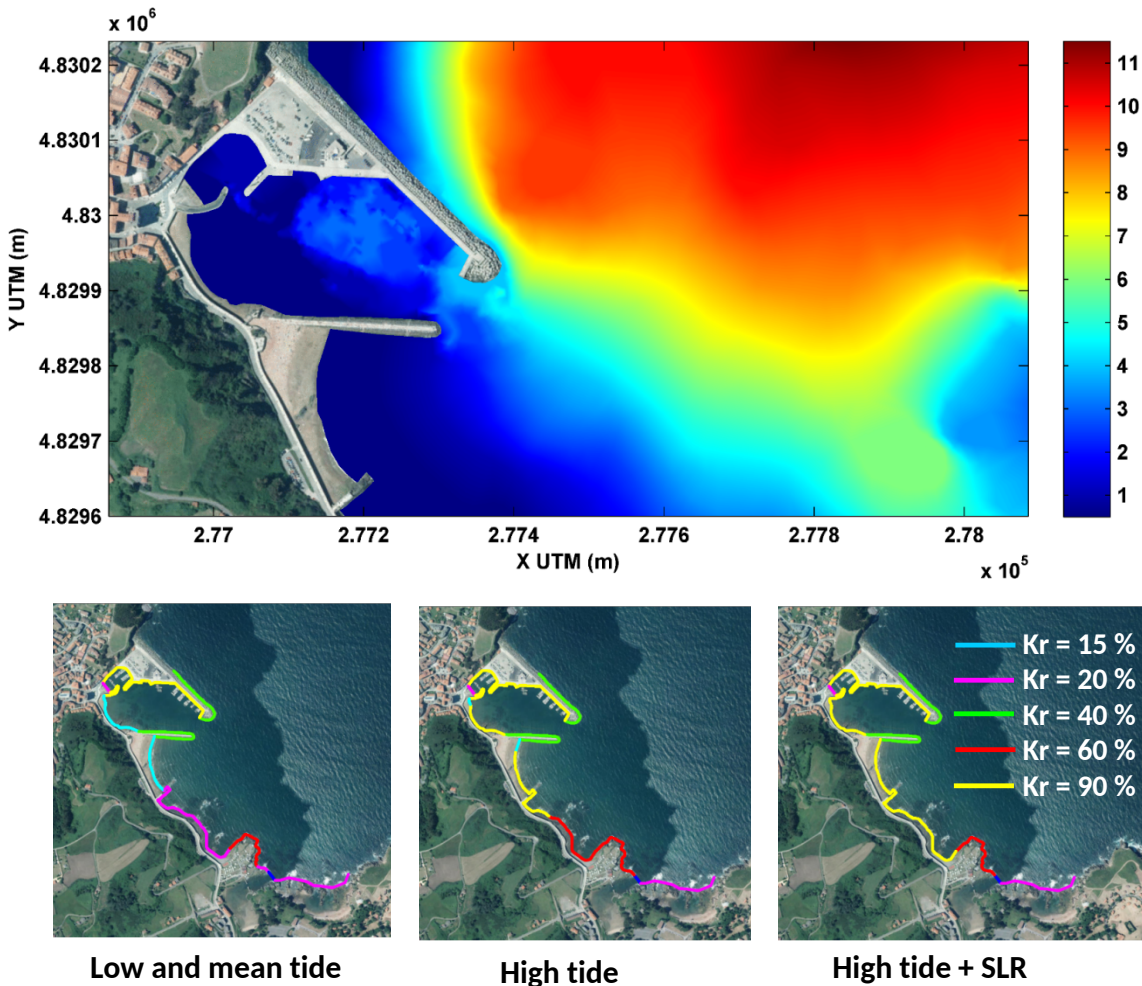
152 The Port of Candás (43° 35, 3' N; 5° 45, 5' W) is located in the region of Asturias (~~which is~~
153 ~~located in~~ northwest Spain), ~~and~~ bordered ~~to the north~~ by the Cantabrian Sea ~~to the north~~. The
154 current port land area is over 41.150 m² with a ~~72 m~~ berthing length ~~of 72 m~~. The ~~port's~~ main
155 activities ~~of the port~~ are fishing and recreation (see Figure 1). The water depth in the inner harbor
156 varies between 1 and 3 m (Figure 2). ~~Figure 2 shows the bathymetry of the harbor area.~~ The main
157 breakwater has a trapezoidal cross-section ~~consisting of built of~~ an outer layer of 23 tons concrete
158 cubes, a secondary layer with 2-3 tons ~~of~~ gravel, a 50-1000 kg rubble layer and a core. A concrete
159 crown wall ~~lies is located~~ on ~~the~~ top of the rubble mound breakwater with ~~its~~ crest level ~~of at~~
160 11.50 m. The geometry and materials of the different natural and artificial structures of the port's
161 inner boundaries ~~causedetermine thatchanges in~~ wave reflection ~~changes~~ along these boundaries
162 ~~atfor~~ different water levels. ~~In/For~~ this ~~approach/ case study??~~ these variations ~~wereare~~ included
163 in the agitation modelling by using different reflection coefficients along the berths and docks for
164 the four sea levels considered (see Figure 2). ~~Specifically, the following reflection coefficients~~
165 ~~werehave been considered, according to the typology they represent: dissipative beach (Kr=0.15),~~
166 ~~reflecting beach (Kr=0.20), rubble-mound breakwater (Kr=0.40), cliff (Kr=0.60) and vertical~~
167 ~~wharf (Kr=0.9).~~ For low and mean tide reflection coefficients ~~wereare~~ kept constant.



168
169

Figure 1. Location of the Port of Candás in northernat the north of Spain.

170



171

172 **Figure 2.** Upper figure: Bathymetry of the study area ~~area of study~~ (depth in meters). Lower
 173 figures: Reflection coefficients adopted/~~reached?~~ along the port boundaries under different sea
 174 levels: low and mean tide, high tide and high tide + SLR. $K_r=0.15$ for dissipative beach, $K_r=0.20$
 175 for reflecting beach, $K_r=0.40$ for rubble-mound breakwater, $K_r=0.60$ for cliff and $K_r=0.9$ for
 176 vertical wharf.

177

178 3 Databases

179 Sea level pressure fields of the Climate Forecast System Reanalysis (CFSR and CFSRv2; [24])
 180 ~~were are~~ used to define the predictor of the statistical models ~~to be~~ explained in section 4. The
 181 temporal coverage spans neds from 1979 to 2013, with an hourly temporal resolution and a 0.5°
 182 spatial resolution.

183 The historical wave information used ~~in this work is was~~ the high resolution coastal wave database
 184 Downscaled Ocean Waves (DOW, [25]), with a low resolution mesh ~~resolution~~ of $0.01^\circ \times 0.008^\circ$

185 ~~(low-resolution meshes), and with~~ several nested meshes reaching a maximum resolution of 200
 186 m. This database ~~was~~ generated using a hybrid downscaling methodology which combines
 187 statistical techniques and dynamical simulations. The Global Ocean Waves database (GOW, [26])
 188 ~~at a regional scale was~~ used ~~at the regional scale~~ as wave forcing to generate the coastal wave
 189 reanalysis. The SeaWind database, generated ~~by~~ performing a dynamical downscaling of the
 190 NCEP/NCAR wind reanalysis at a spatial scale of 30 km [27], ~~was~~ used as wind forcing. ~~The~~
 191 ~~results of these procedures/models/analyses~~ ~~Outputs~~ ~~provided~~ ~~the following~~ hourly sea state
 192 parameters from 1948 to 2014: significant wave height (H_s), mean period (T_m), peak period (T_p)
 193 and wave direction (θ).

194 The 62-year (1948–2014) high-resolution hindcast of the meteorological sea level component
 195 (storm surge, SS) (GOS 1.1; [28]) ~~was has been~~ used ~~to determine for the~~ historical storm surge
 196 data. ~~The~~ GOS 1.1 database ~~was has been~~ developed for Southern Europe using the Regional Ocean
 197 Model System (ROMS) with a horizontal resolution of $1/8^\circ$ (~ 14 km).

198 The astronomical tide (AT) ~~was~~ reconstructed ~~on an~~ hourly ~~basis~~ at a ~~0.25°~~ spatial resolution of
 199 ~~0.25°~~, using harmonic analyseis ~~on from~~ the outcomes of the global model of ocean tides
 200 (TPXO7.2) that assimilates data from TOPEX/Poseidon missions and tidal gauges for the common
 201 period of waves and storm surge.

202 The regional SLR by 2100 for RCP8.5 scenarios ~~was~~ extracted from ~~the~~ global projections of
 203 regional mean sea level ~~values~~ obtained by [29] using a dynamical modeling ~~approach~~ that
 204 incorporates regional contributions of land ice, groundwater depletion and glacial isostatic
 205 adjustment, including gravitational effects due to mass redistribution.

206

207 **4 Methodology and results**

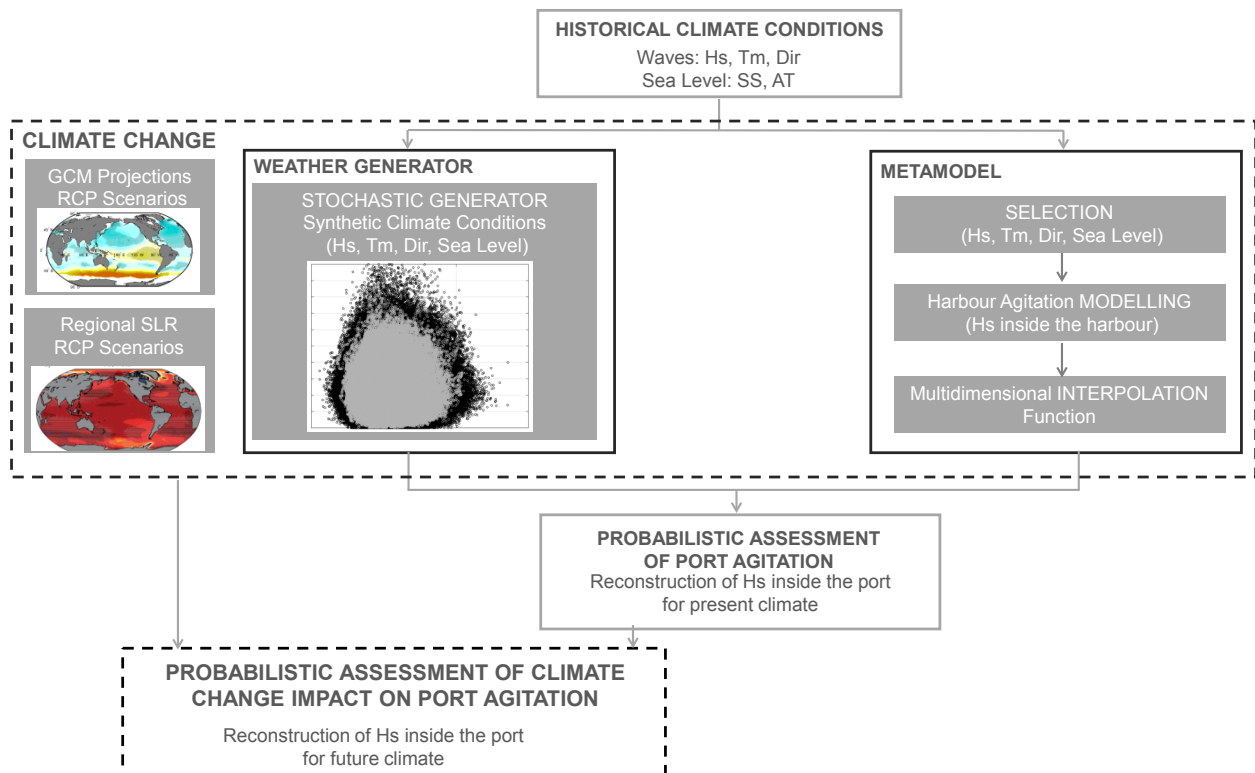
208 The methodology described in Figure 3 is composed of two main parts:

- 209 • A weather generator to derive hourly multivariate marine conditions outside the port.
- 210 • A metamodel to transfer hourly marine conditions outside the port, ~~as~~ generated in ~~the~~
 211 ~~previous step~~, to the inner harbor, in order to obtain wave agitation.

212 The definition of the stochastic generator requires historical information of the forcing conditions
 213 outside the port. The climate emulator based on weather patterns for modelling daily multivariate
 214 events [20] ~~was~~ extended to simulate hourly waves and storm surges at the entrance of the port.
 215 The model is based on a predictor-to-predictand synoptic regression-guided classification [9],
 216 grouping marine conditions according to similar generating meteorological processes, called
 217 weather types (WTs). This method ensures that the predictand within each WT is independent and
 218 identically distributed for the applicability of Gaussian copulas to model the dependence between
 219 variables. Besides, the method captures ~~the climate's~~ non-stationary characteristics ~~based on by~~
 220 ~~means of~~ the variability of WTs over time. A Monte Carlo approximation is applied to
 221 stochastically simulate large samples of hourly conditions at the entrance of the harbor.

222 For the second step, a metamodel based on a hybrid downscaling methodology (a combination of
 223 dynamical and statistical downscaling) developed to generate high resolution nearshore wave
 224 reanalysis databases [25] was adopted. Specifically, A number of representative sea states was
 225 propagated using a model solving the elliptic mild slope (MSP, [30]) and the time series
 226 reconstructed of nearshore waves were reconstructed by means of an interpolation technique. The
 227 way in which the number of simulations was selected from the synthetic data ensureds the
 228 coverage of the new multivariate space of climate drivers. The probabilistic assessment of current
 229 port operability due to wave agitation was obtained by reconstructing the significant wave height
 230 inside the port for each simulated hourly condition at the entrance of the harbor for the present
 231 climate.

232 To assess climate change impacts on port agitation, climate change can be introduced in the
 233 weather generator by means of future WT probabilities that can be reflected as changes in waves
 234 and storm surges and SLR added to the sea level time series of sea level. The metamodel has to be
 235 updated to take into account climate change in the osee cases selected to be modelled as well as the
 236 effect of SLR on the reflection coefficients to be used in the wave agitation model.



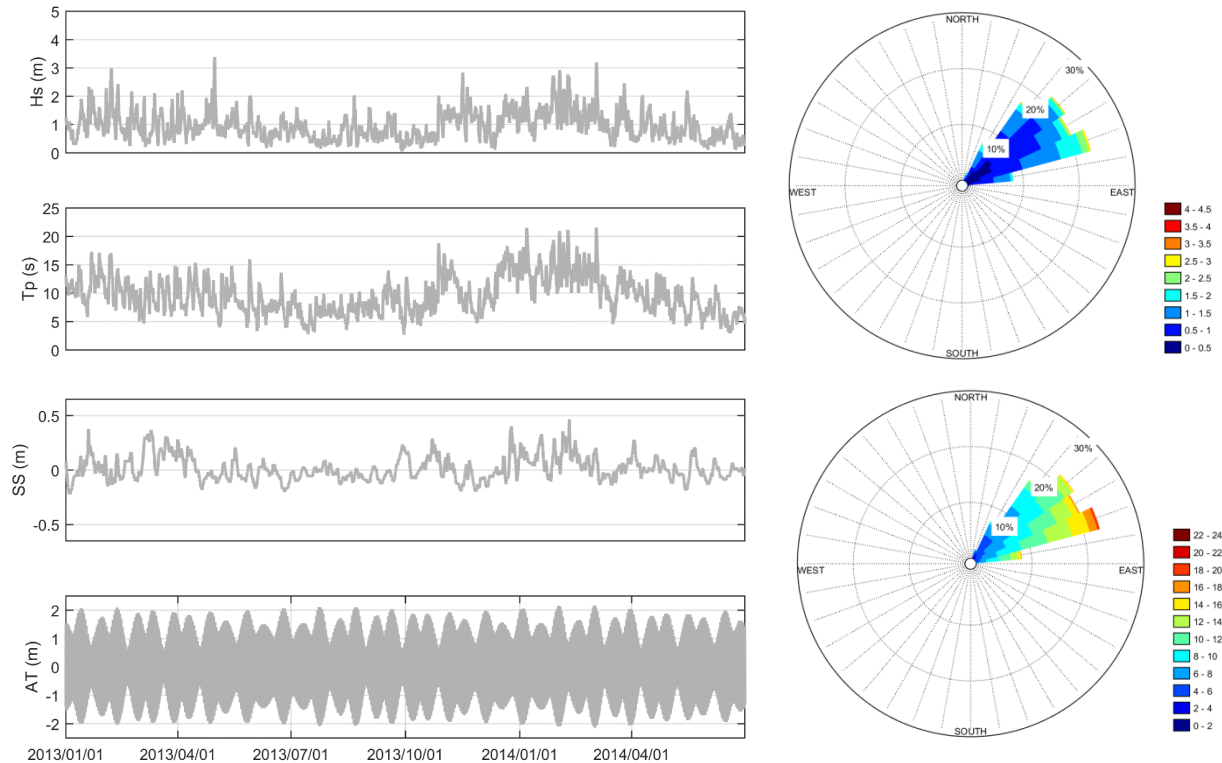
237

238 **Figure 3.** Probabilistic methodology which combines a weather generator and a metamodel to
 239 asses port operability due to wave agitation under present and future conditions.

240

241 Figure 4 shows the time series for years 2013 and 2014 and the distribution of $H_s-\theta$ and $T_p-\theta$ of
 242 the forcing conditions occurring outside the port, obtained from the databases described in section
 243 2. Forcing these conditions are defined outside the port were defined at about 6.0 m depth. Wave
 244 climate at this location has suffered an intense refraction due to the protection effect of Cape Peñas

245 (Figure 1) resulting in wave energy concentration in the N-E sector. The maximum significant
 246 wave height is limited to 4.5 m while peak periods reach values of 20 s which can be combined
 247 with storm surges of almost 0.5 m and with high spring tides over 2.0 m.



248

249 **Figure 4.** H_s , T_p , SS and AT values for two years within the time series Example of two years of
 250 time series (H_s , T_p , SS and AT) at the entrance of the harbor (left panels). H_s and T_p roses (right
 251 panels).

252

253 4.1 Weather generator

254 A weather-type framework was used to model the nonstationary behavior of the local
 255 multivariate predictand (H_s , T_m , T_p , θ and SS) related with large-scale predictors (sea level
 256 pressure, SLP). The daily predictor was classified into a discrete number of weather patterns
 257 (WTs) according to their synoptic similarity. The hourly multivariate events were modelled
 258 using a marginal distribution for each predictand variable and a Gaussian copula within each WT.
 259 The stochastic generator follows is composed of similar steps as to the one developed by [20] for
 260 multivariate extremes, except in this case the extremal index is not required. The five steps
 261 involved in this model are: 1) To collect and pre-process historical data of the predictor (sea level
 262 pressure, SLP) and predictands (H_s , T_m , T_p , θ and SS). 2) Define WTs weather types using a semi-
 263 guided classification [31]. 3) Fit a stationary model (e.g. Lognormal, Generalized Extreme Value)
 264 to each variable of the multivariate predictand (H_s , T_m , SS outside the port) associated with each
 265 WT weather type. 4) Model the dependence between predictand variables within each weather type

266 using a Gaussian copula. 5) Generate synthetic multivariate hourly conditions taking into account
 267 the monthly WT probability and dependence structure associated with each WT.

268 The spatial domain of the predictor should cover the oceanic region responsible for generating
 269 of waves arriving at each location of interest. The temporal coverage (recent history) should
 270 account for the wave travel time from generation to the target location. Based on previous works,
 271 The semi-supervised WTs of the grid node from the global collection of WTs at a $1.0^\circ \times 1.0^\circ$
 272 resolution, generated to obtain global wave projections [9], at a location closest to the study port
 273 of study, was used to develop the weather generator (steps 1 and 2 in this section). The predictor
 274 definition (spatial domain and temporal coverage) corresponded to the subdomain covering which
 275 covers the North Atlantic Ocean (from an ocean the division of the ocean based on a global wave
 276 genesis characterization). The predictor was defined as the 3-daily mean SLP and 3-daily mean
 277 SLPG (squared SLP gradients), calculated daily throughout the historical time period. More details
 278 regarding about this characterization and the WT collection can be found in [9]. A regression
 279 guided classification was applied to a combination of the weighted predictor and predictand
 280 estimations from a regression model linking the SLP fields with local marine conditions. The level
 281 of influence of the wave and storm surge data was controlled by a simple weighting factor which
 282 balances the loss/gain of predictor/predictand representativeness. A factor equal to 0.6 was
 283 implemented based on previous sensitivity analyses. A better grouping of the predictand was
 284 obtained due to a stronger relation of the WTs with the local marine climate conditions.

285 The long-term marginal distributions (step 3) of hourly H_s , T_m , and SS outside the port within each
 286 WT were fitted to a generalized extreme value (GEV) distribution, a Lognormal distribution
 287 or Unified Distribution Model [32], obtaining the best fit of the central regime with a GEV. The
 288 empirical distribution was used for the wave direction variable. A heteroscedastic model
 289 between T_p and T_m was fitted within each WT. T_p was considered to be normally distributed
 290 with parameters mean and variance being a function of T_m (polynomials with unknown degree). A
 291 Gaussian Copula was used to model the dependence between H_s , T_m , SS and θ (step 4).

292 The Monte Carlo sampling procedure used to generate synthetic marine conditions (step 5)
 293 requires the following phases: i) Sample a daily WT from a Generalized Bernoulli distribution due
 294 to the categorical choice of one of the $N=100$ WTs. ii) Randomly generate randomly 24 hourly
 295 synthetic H_s , T_m , θ and SS using the Gaussian copula and the marginal fits associated with the daily
 296 simulated WT; iii) Sample 24 hourly T_p from the heteroscedastic model between T_p and T_m
 297 associated with the daily WT; iv) Independently sample 24 hourly values of astronomical tide from
 298 its monthly empirical distribution. The process is repeated until a synthetic 90-year time series of
 299 90-years hourly time-series-of multivariate forcing marine conditions is obtained.

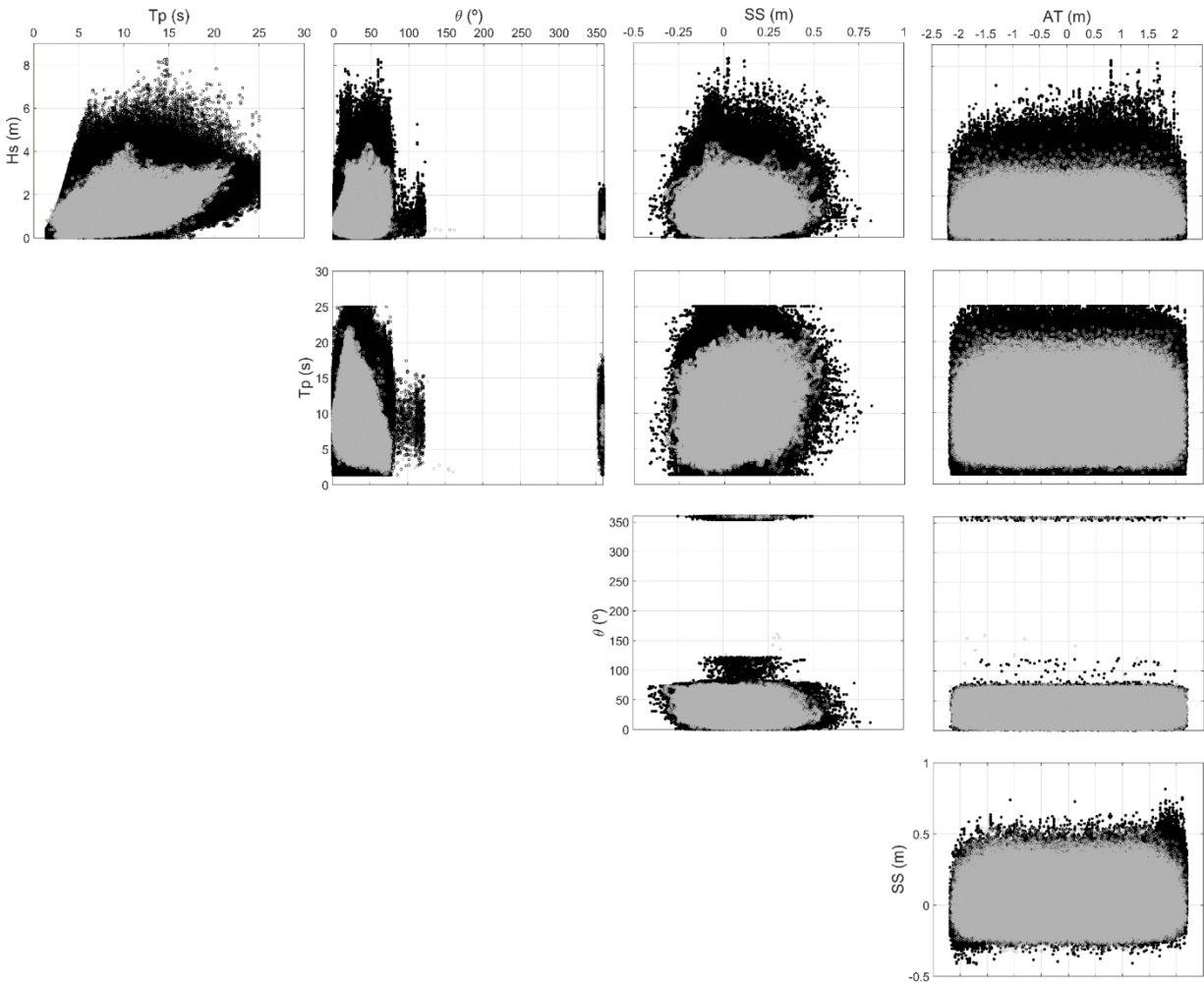
300 One thousand, 90-year long, new time series of H_s , T_m , T_p , θ , SS and AT were simulated with
 301 the emulator—previously fitted emulator. Each series was generated with a different set of
 302 parameters, randomly taken from the parameters sample obtained considering a Gaussian
 303 distribution. Scatter plots of the five sea-storm variables are shown in Figure 5. Monte Carlo
 304 simulations (1000 samples of 50 years of hourly data, comparable to their order to compare with
 305 50 years of historical data period) are shown as grey dots and historical data as black dots. The
 306 large multivariate sample of hourly forcing conditions captures the characteristics of dependencies
 307 among between the variables. Wave breaking and wave steepness limit the M maximum simulated
 308 wave height is limited to 5.0 m and maximum simulated wave period was is limited to 25 s.

309 The effect of [the imposed](#) physical limitations of wave slope [imposed](#) can be observed in the
 310 correct reproduction of the relation between wave heights and small wave periods. Figure 6 shows
 311 the joint probability density functions of (H_s, T_p) , (H_s, θ) , (H_s, SS) and (T_m, T_p) obtained from the
 312 historical series (blue lines) and from the simulated series (dashed lines). The simulated series are
 313 able to reproduce the main features of the original bivariate distributions. They fail in representing
 314 some details of the distributions, as the [clearer](#) dependence between wave heights around 1.0
 315 m and low peak periods.

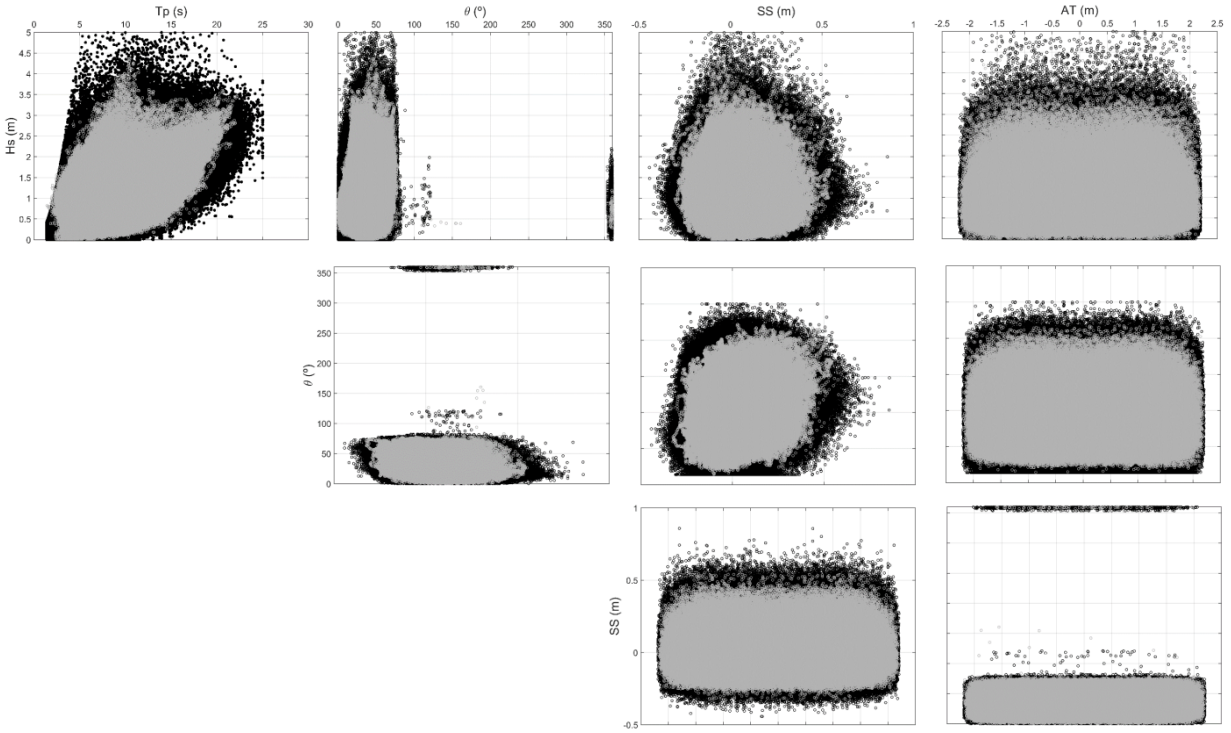
316

317

318



319

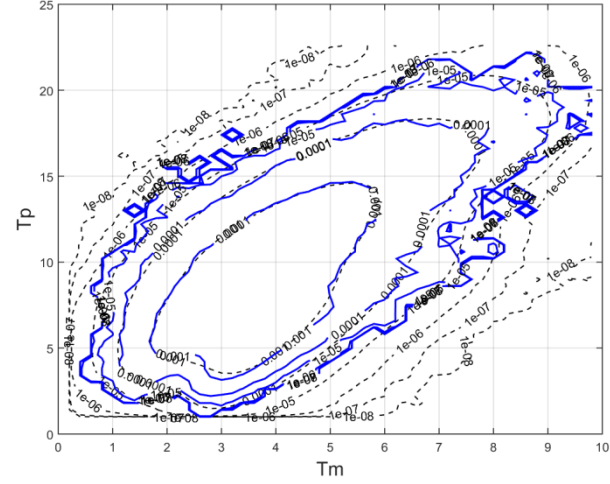
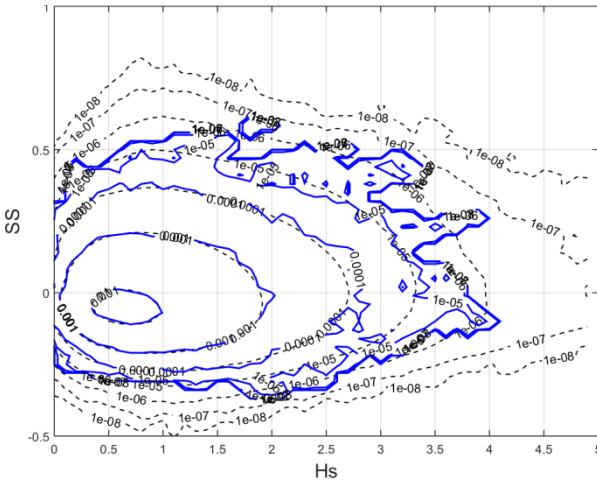
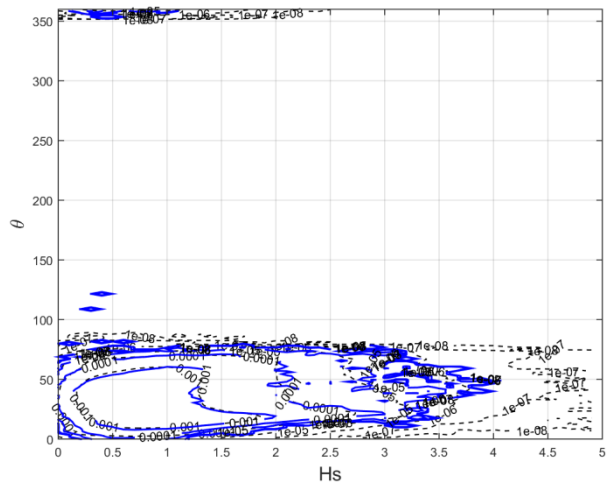
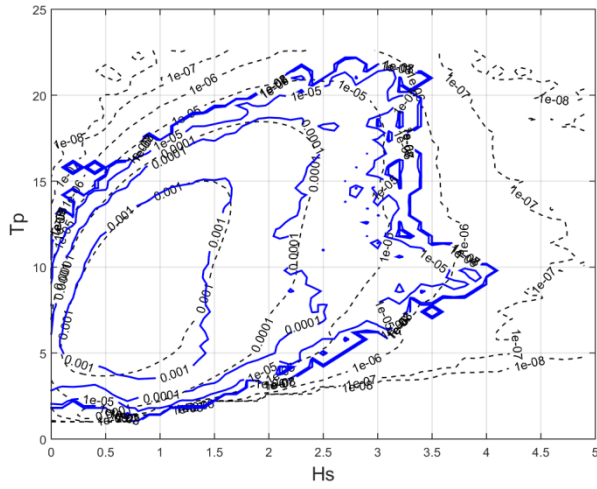


320

321 **Figure 5.** Scatter plots of marine climate (H_s , T_p , θ , SS , AT) at the entrance of the port. Historical
 322 data: ~~black-grey~~ dots; Monte Carlo simulations (1000 samples of 50 years of hourly data) ~~simulated~~
 323 data: ~~grey-black~~ dots.

324

325



----- Simulations (1000x50 years)

——— Observations (1000x50 years)

326

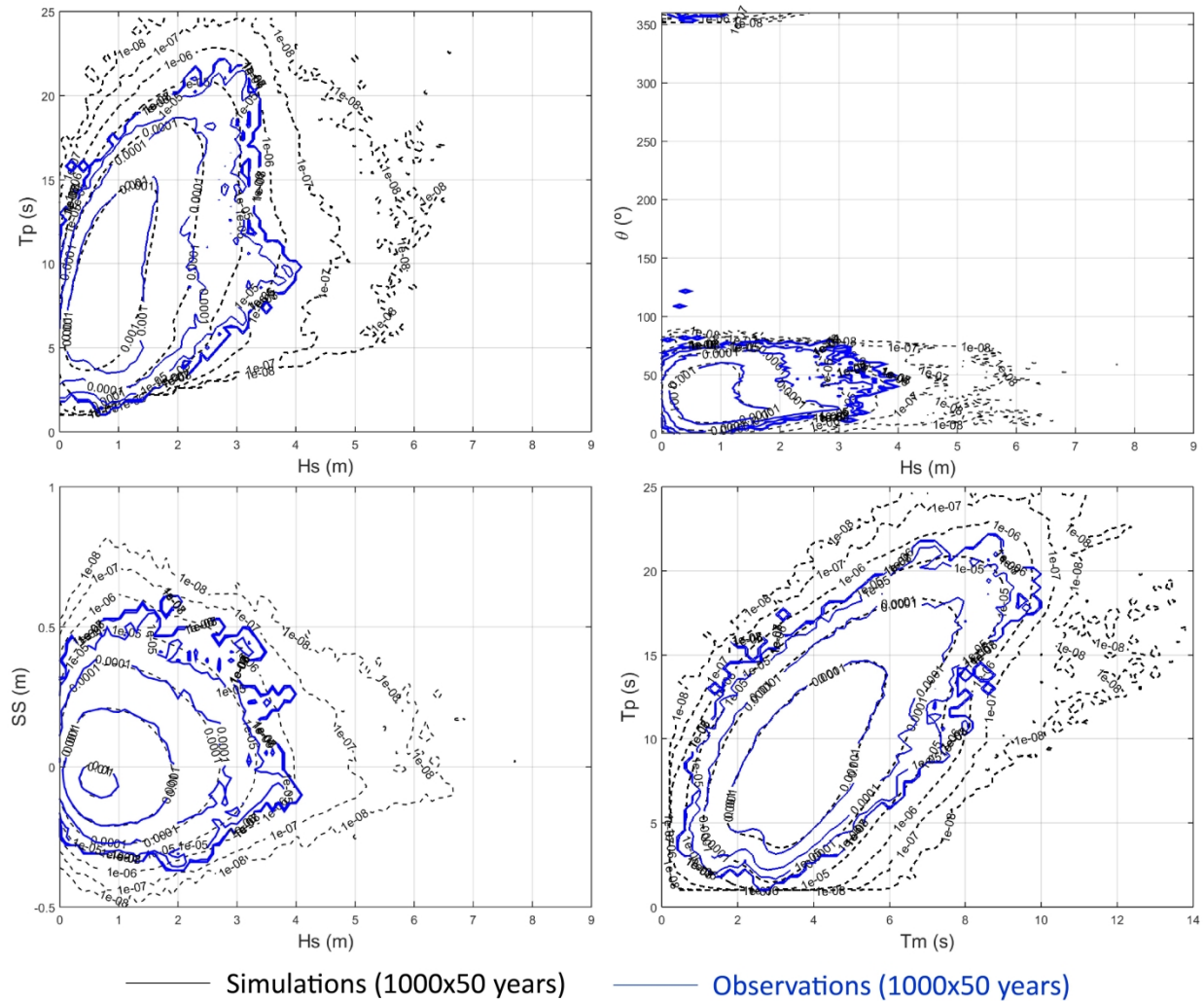
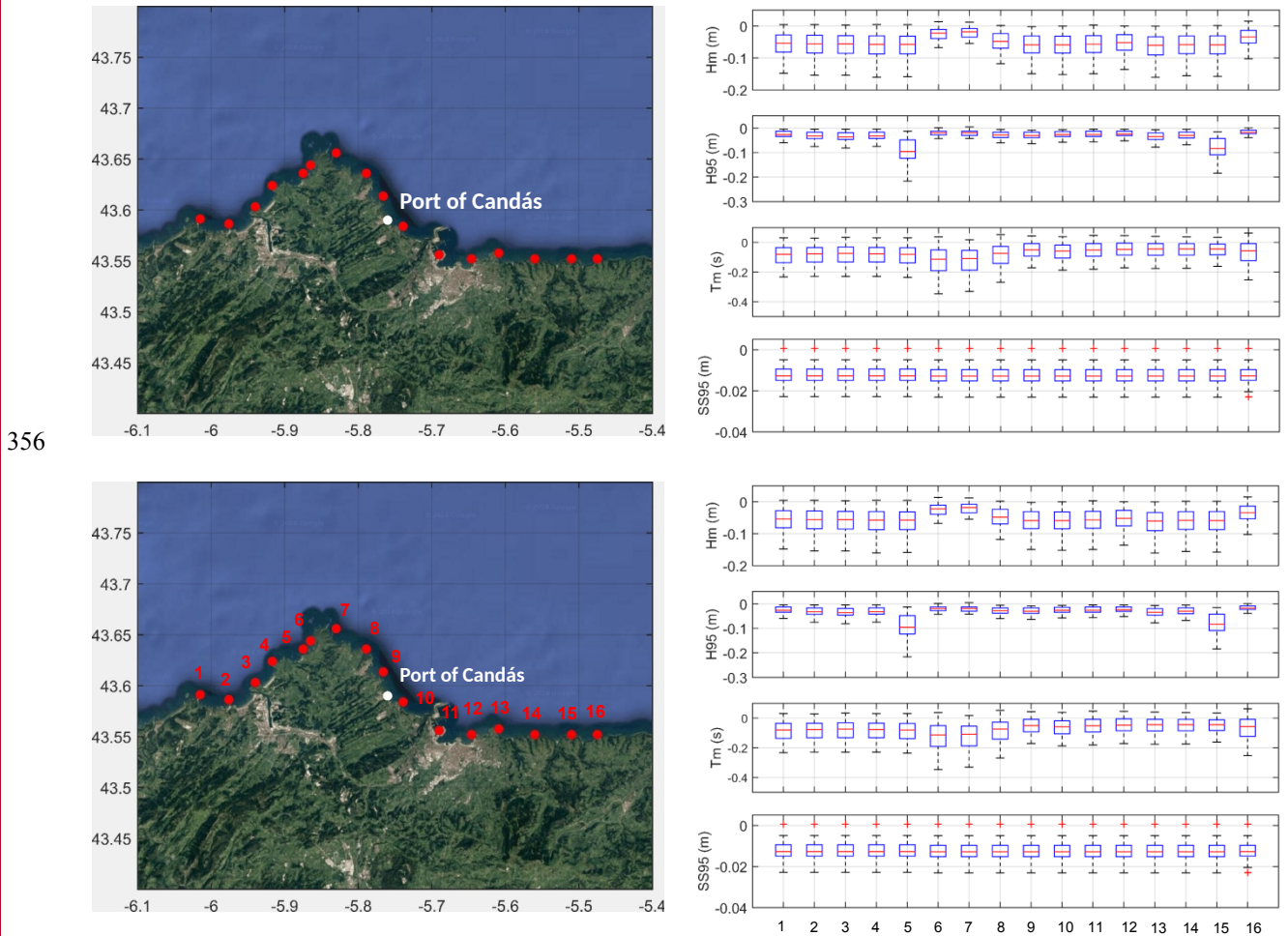


Figure 6. Joint probability density function of the hourly forcing conditions. Blue solid lines represent the results obtained from the historical data and black dashed lines represent the simulated data generated using the weather generator.

Regarding future synthetic time series in a future period (e.g. in the period; 2010-2100), climate change can be introduced taking into account changes in the storminess by means of future WT probabilities from GCMs and the increase in the mean sea level. Robust multi-model ensemble projections at high spatial resolutions ($0.01^{\circ} \times 0.008^{\circ}$ using DOW at the reference database) measured over the whole century (2010–2099) were estimated along the northern coast of Spain [33]. Future wave and storm surge projections were statistically downscaled using a weather-type approach [34] for the same 40 GCMs as in the regional wave projections made in Europe [35]. The statistical relationship was established as similarly into the first steps of the weather generator. In this case, however, the empirical probability distribution of each sea state parameter (e.g., significant wave height) associated with each WT was calculated. The distribution of this variable for a certain time period can be estimated as the sum of the probability of each WT during that period multiplied by the corresponding empirical distribution. Different statistics (e.g., mean, 95th percentile) can be derived from the estimated distribution. One of the advantages of this

345 statistical downscaling methodology is that the scale representativeness of the projections depends
346 on the underlying historical wave databases used as a reference [9]. Figure 7 shows the multimodel
347 ensemble projections of the annual mean and the 95th percentile of the significant wave height, the
348 mean period and the 95th percentile of ~~the~~ storm surge in the area surrounding around the study
349 port for the ~~time~~ period 2070–2099 compared with ~~respect to the~~ 1979–2010 period under the
350 RCP8.5 scenario. Box plots illustrated inform about the uncertainty inherent in of the future
351 changes obtained from the 40 GCMs. The outcomes reveal slight decreases in surges and wave
352 heights and periods. These changes are assumed to be negligible compared to with the effect of the
353 SLR in the wave propagation inside the port. ~~Indeed Moreover,~~ the decreasing waves and storm
354 surge resulting from according to these expected changes would underestimate the need for the
355 assessment of port operation downtimes. reduce the safety level of the port exploitation.



358 **Figure 7.** Regional multimodel projections (RCP8.5, 2070–2099 with respect to 1979–2005) for
 359 the mean and the 95th percentile of ~~the~~ wave significant wave height, the mean wave period and
 360 the 95th percentile of ~~the~~ storm surge along the coastline surrounding around the study port.

361

362 Following the approach proposed by [36] to account for the SLR uncertainty around SLR in the
 363 assessment of flooding risk, a lognormal distribution was fitted with the mean and standard
 364 deviation of the from-regional projections produced by [29] for the RCP8.5 scenarios in 2100 (i.e.,
 365 0.63 ± 0.20 m at the study area) for the RCP8.5 scenarios. The Lognormal distribution is
 366 considered as the most likely distribution representing future sea level rise/SLR [37], although
 367 increased rates of ice sheet loss are/were not included in this study. The deciles from fitted
 368 lognormal distributions split the SLR data set in from each horizon year into ten equally probable
 369 parts with equal probability, being the 2100 deciles being: 0.377 m; 0.454 m; 0.507 m; 0.553 m;
 370 0.599 m; 0.646 m; 0.699 m; 0.763 m; 0.852 m; and 1.025 m, respectively. Ten curves were
 371 derived from the-local RCP8.5 SLR values in 2025, 2050 and 2100 using a second order
 372 polynomial function in order to adopt the shape of those provided by the from-IPCC [38]. Hourly
 373 SLR time series (2010-2100) derived from these curves were added to the synthetic sea level

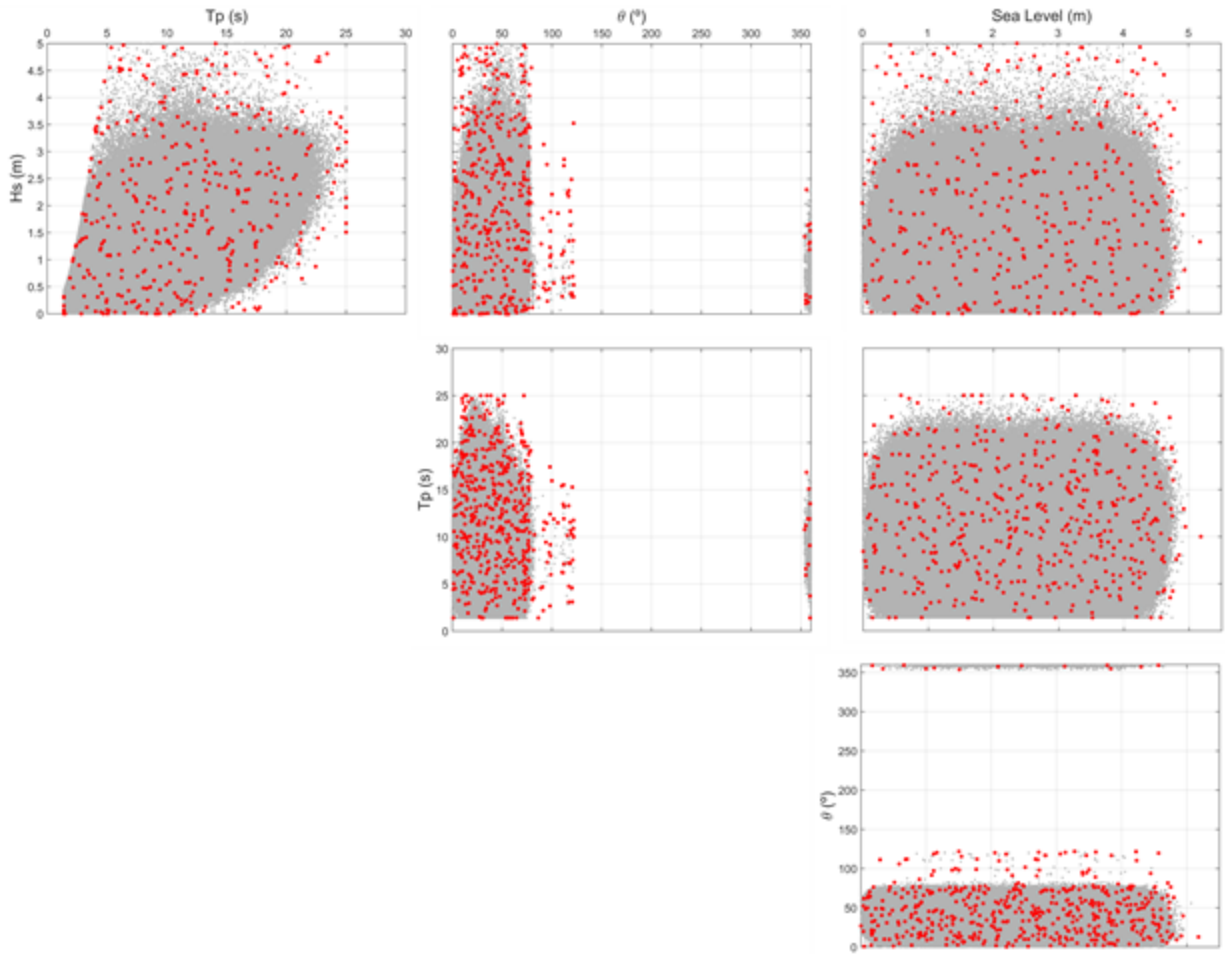
374 time series (defined as the sum of storm surge and astronomical tide) to define ~~the~~ future forcing
 375 conditions of port agitation.

376

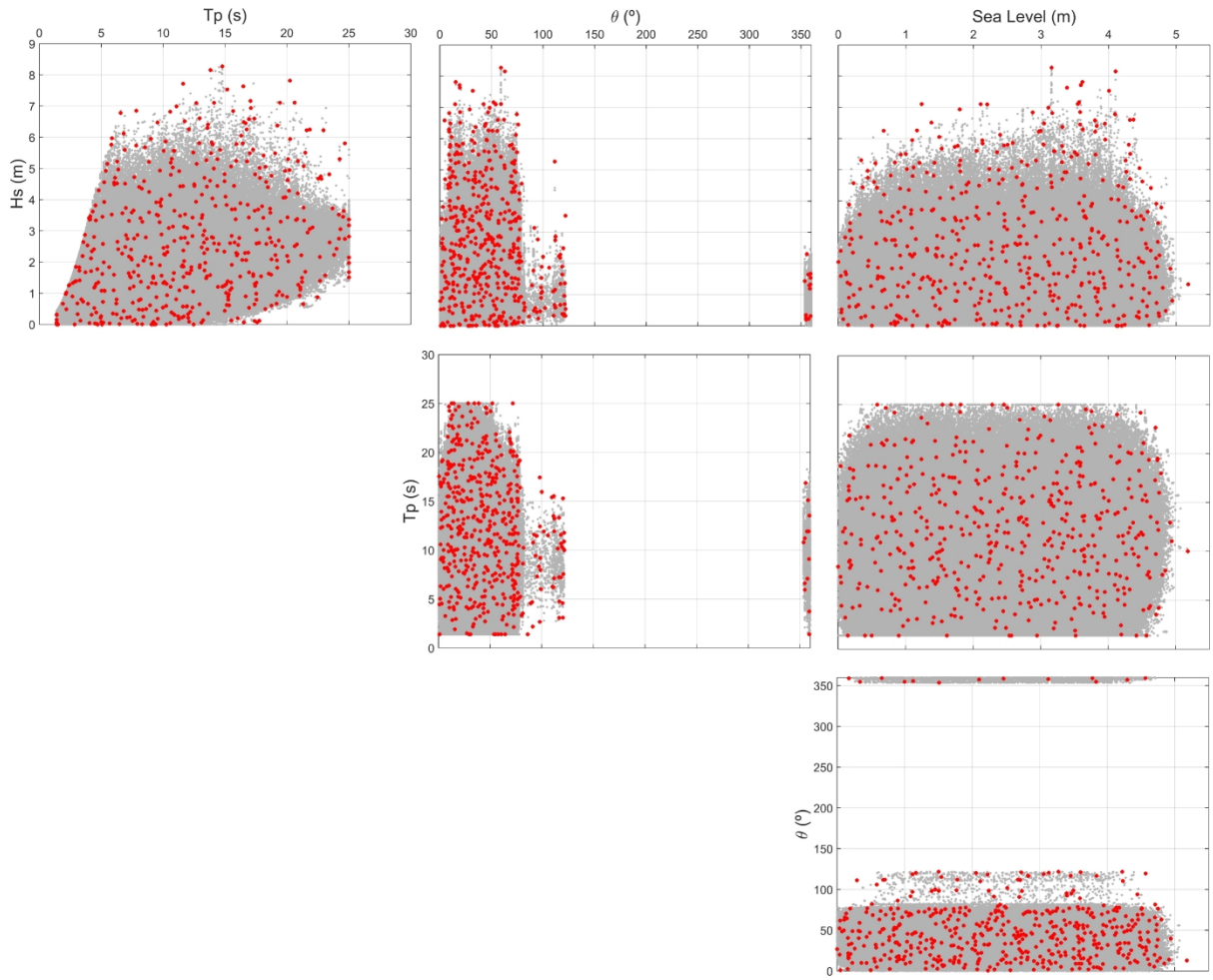
377 4.2 Metamodel

378 The steps followed to define the metamodel used to transform all the synthetic forcing conditions
 379 outside the port ~~were~~are: 1) selection of a limited number of cases comprising ~~which are~~ the most
 380 representative scenarios of waves and sea level fluctuations (storm-surge, astronomical tide and
 381 sea level rise) outside the port; 2) a wave agitation strategy to propagate the selected sea states
 382 from the entrance of the bay towards the inner harbour zone; 3) reconstruction of the time series
 383 of significant wave heights inside the port.

384 A subset of sea states ($M=500$) representative of ~~the~~ marine conditions outside the port was
 385 selected using the maximum dissimilarity algorithm (MDA, [12]). The MDA identifies a subset
 386 comprising the most dissimilar data in a database. The selection starts by initializing the subset
 387 through the transference of one vector from the data sample. The remaining ~~st~~ of the elements are
 388 selected iteratively, transferring the most dissimilar one from the remaining data in the database to
 389 the subset. - Figure 8 shows the distribution of the selected subset from the MDA (~~larger red dots~~)
 390 over the full multivariate parameter space (H_s , T_p , θ and sea level) covered by the Monte Carlo
 391 realizations (~~grey dots~~). The multivariate subset is distributed evenly across the space covering the
 392 potential combinations between the four variables with some points selected in the outline of the
 393 data space, which contributes to an accurate reconstructions of wave agitation conditions inside
 394 the port using the proposed metamodel.



395



396

397 **Figure 8.** Scatter plots of simulated data (grey dots) and the selected cases using the MDA (red
 398 dots ~~in red~~).

399

400 The MSP numerical model [30] wasis used for wave agitation simulations. This model is able to
 401 solve ~~the~~ wave propagation towards and into the harbor, taking into account ~~the~~ refraction,
 402 diffraction, wave breaking and partial reflection imposed by ~~the~~ natural and artificial structures
 403 (quays, basins, breakwaters, etc.) and real bathymetry contours. The model provides (2DH)
 404 significant wave maps along the whole numerical domain. A complete spectral sea-state
 405 propagation strategy [389] based on the invocation of a pre-calculated monochromatic wave
 406 catalogue wasis applied to noticeably reduce the CPU-effort to propagate real wave spectra
 407 towards any inner control point. This technique is based on a three-step method:

408 1. The selection of N monochromatic wave conditions (the combination of periods T and
 409 directions ??) by collapsing the 4D-hypermatrix [frequency, direction, energy, time] for the whole
 410 wave hindcast used, into a single resulting matrix representings the historical energy packs
 411 available in the study zone (for a typical 35 frequency x 72 direction spectrum matrix, and taking
 412 into account real/theoretical frequency and direction spreading factors for each hour). N can adopt

413 values from 30% to 60% of the total matrix size used, depending on the geographical location of
 414 the harbor/ outer wave climate.

415 2. The numerical propagation of each N monochromatic waves (using a constant wave height
 416 H, because of the linear nature of the model used) and for the different sea levels considered.

417 3. The aggregation of any spectrum by adding all the individual energy packs that defines it.

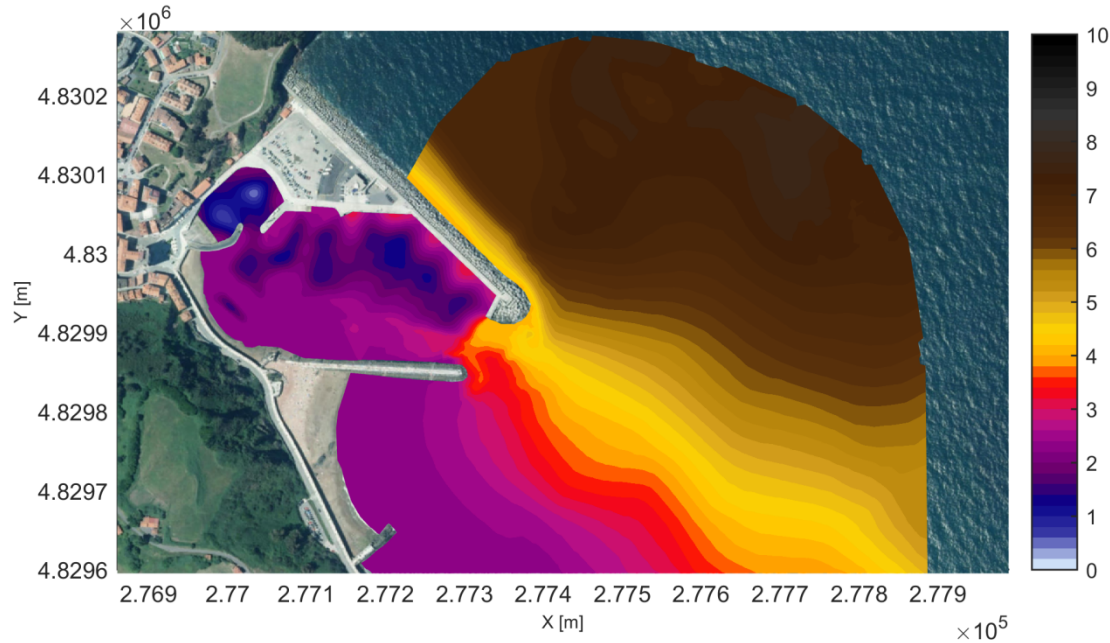
418 For this study additional considerations were established:

419 4. Four water levels were used (total Nx4 monochromatic cases) (three to cover the
 420 astronomical tide range and one as expected upper SLR).

421 5. Changes in reflection coefficients in the model's setup (as described in the study area
 422 section) due to SLR.

423 Monochromatic wave conditions, covering all wave periods and directions physically available at
 424 the entrance of the bay, are propagated inside the port using the MSP model at four water levels
 425 (to cover the astronomical tide range and an expected upper sea level rise). Changes in reflection
 426 coefficients due to SLR are implemented in the wave model setup (as described in the study area
 427 section). For each of the real sea state conditions selected, wave agitation inside the port is
 428 reconstructed by linear superposition of the results corresponding to monochromatic waves and
 429 linear interpolation at the corresponding sea level.

430 This technique, besides achieving a radical CPU-time reduction, enables to rapidly include any
 431 future scenario needed or sensitivity analysis required, as well as changes in one or many spectrum
 432 variables due to climate change (energy, frequency, direction and its frequency-directional
 433 spreading). On the other hand, this technique could over-predict wave-shoaling effects, especially
 434 for shallow bathymetry zones. Thus, it should be used with caution if non-linear wave-wave
 435 interactions are expected in the study zone, especially for wave breaking related processes and
 436 shoaling. This drawback is minimized for open harbors, with (in general) quasi-constant/ mild
 437 bathymetry configurations within the basins and outer zones, as showned in [39]. Figure 9 shows
 438 an example of a wave agitation map inside the port for conditions outside the port defined by
 439 $H_s=7.2$ m; $T_p=15.8$ s; $\theta =54.5^\circ$ and sea level=3.63 m.



440

441 **Figure 9.** Wave agitation map for the following marine conditions outside the port: $H_s=7.2$ m;
 442 $T_p=15.8$ s; $\theta =54.5^\circ$ and sea level=3.63 m.

443 The significant wave height time series inside the port are reconstructed using the
 444 multidimensional interpolation technique of radial basis functions (RBF, [3940]). The RBFs
 445 enable a statistical relationship to be defined between the marine parameters characterizing the
 446 forcing conditions and the wave height inside the port from the results of the selected cases. The
 447 RBF interpolation method defines the function to be approximated by means of a weighted sum
 448 of radially symmetric basic functions located at the data points where the results are available. A
 449 more detailed description of these statistical tools implemented in the proposed hybrid
 450 methodology can be found in [12].

451

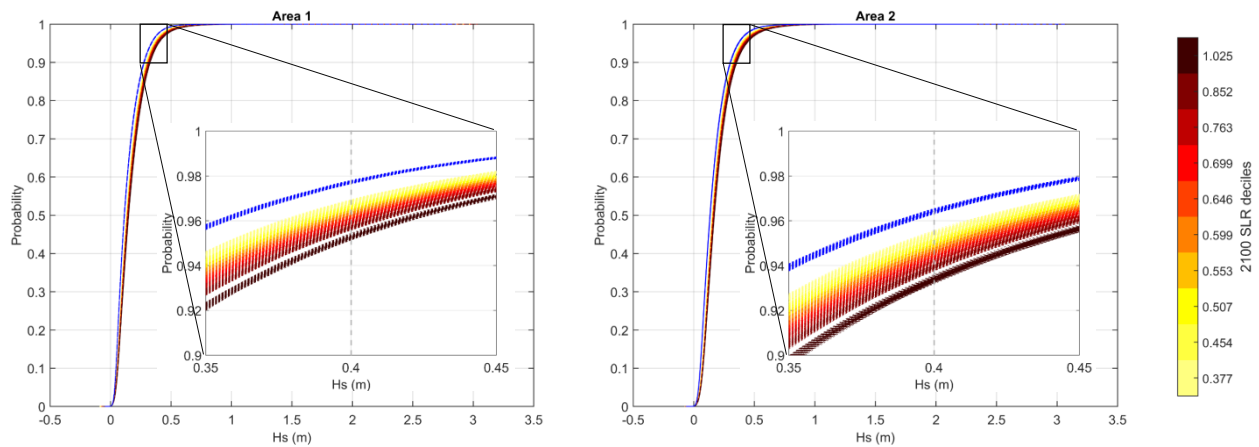
452

4.3 Results

453 The synthetic historical time series of marine conditions (waves, storm surge, and astronomical
 454 tide) outside the port ~~were~~ transferred inside the port using the corresponding RBF. The
 455 synthetic time series outside the port ~~was~~ transformed to the future period 2010-2099 adding
 456 ~~the corresponding??~~ SLR to each hourly sea level. Their corresponding wave height inside the port
 457 ~~was is~~ reconstructed applying the RBF.

458 The annual operability or the hours of non-operability ~~are is some one~~ of the basic port design
 459 criteria ~~for ports stipulated given~~ by national and/or international standards (such as ROM or
 460 PIANC). In this example, hours of non-operability ~~were~~ calculated from each time series as the
 461 hours exceeding a certain threshold of H_s inside the port. Here, A threshold equal to of 0.4 m was is
 462 applied, as suggested in the Spanish Recommendations for Maritime Structures for Fishing Ports
 463 (ROM 3.1-99, [4041]).

464 Figure 10 shows the historical and future empirical cumulative distributions of significant wave height, H_s , inside the port in Areas 1 and 2 from the one thousand synthetic time series. Fifty-
 465 year long time series of forcing conditions ~~were~~ considered in the assessment of the port's
 466 downtimes ~~since because~~ the useful life of the Port of Candás is established in 50 years. The future
 468 distribution ~~was~~ based on the thousand synthetic future hourly time series from 2050-2099
 469 obtained for the ten SLR scenarios sampled from a lognormal distribution of the RCP8.5 SLR
 470 projections. The future empirical distributions for the ten SLR scenarios ~~were~~ represented in a
 471 yellow-red scale corresponding to the lowest-~~to the~~ highest decile, ~~respectively~~. The probability
 472 of a significant wave height lower than 0.4 m (non-operability threshold for fishing ports) is lower
 473 ~~the higher the as the~~ SLR is higher (see the zoomed image of the empirical cumulative distribution
 474 between 0.35 to 0.45 m in Figure 10).



475

476 **Figure 10.** Historical empirical cumulative distribution (in blue) and future empirical cumulative
 477 distributions for the ten SLR scenarios (in yellow-red scale) of significant wave height inside the
 478 port in Area 1 and Area 2.

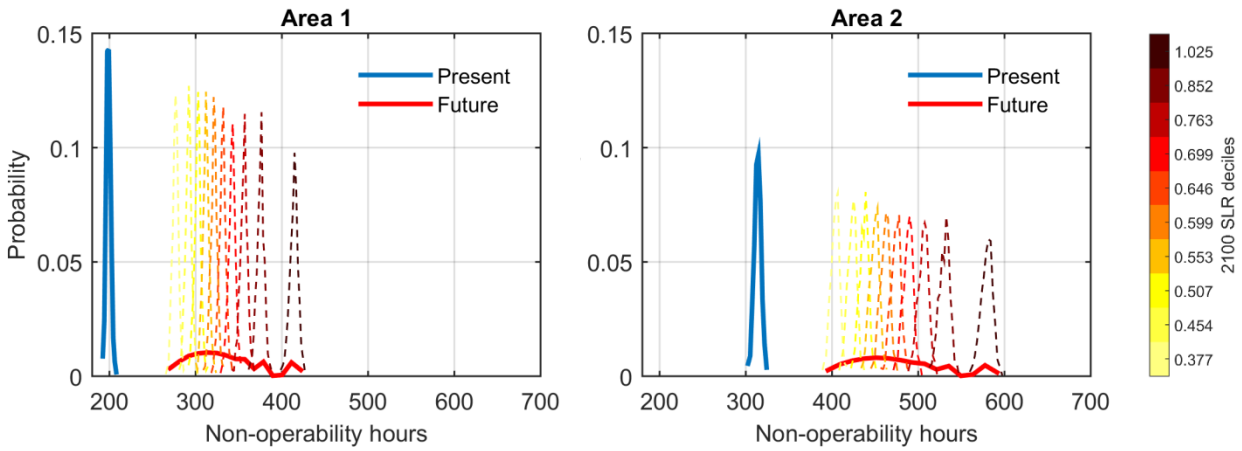
479

480 Hours of non-operability ~~were~~ calculated from the probability (p) obtained for a threshold of
 481 0.4 m as $(1-p) \times 365 \times 24$. The probabilistic distributions of non-operability hours at present (blue)
 482 ~~climate (in blue)~~ and ~~in the future period (2050-2099, (in red)~~ climate conditions are shown in
 483 Figure 11. ~~Future~~ The distributions of non-operability for each RCP8.5 SLR scenario ~~in the future~~
 484 are displayed (dashed lines in the yellow-red color scale) with the ensemble mean future
 485 probabilistic distribution of non-operability (in red). The ensemble mean distribution ~~was~~
 486 obtained ~~by~~ adding up the distribution for each of ~~the~~ ten SLR scenarios multiplied by 0.1 (the
 487 ten SLR scenarios are sampled with an equal probability). It can be noted that hours of non-
 488 operability do increase from present to future ~~conditions~~ for both areas.

489 The probabilistic distribution of non-operability hours ~~under current at present~~ climate ~~conditions~~
 490 represents the uncertainty associated with the historical forcing conditions outside the port. The
 491 ensemble mean future distribution integrates the uncertainty associated with the RCP8.5 SLR
 492 scenarios and the uncertainty due to the forcing conditions outside the port (distributions of non-
 493 operability hours of ten future RCP8.5 SLR scenarios). Besides, ~~higher~~ non-operability hours, ~~as~~
 494 ~~well as a higher uncertainty~~, are expected for higher SLR scenarios, ~~and also a higher uncertainty~~,

495 as it can be observed in wider probabilistic distributions of non-operability hours the higher the as
 496 the SLR decile is higher (see Figure 11).

497
 498



499

500 **Figure 11.** Probabilistic distributions of non-operability hours due to wave agitation in Areas 1
 501 and 2 inside the port in current the present climate (in blue) and in the future (2050-2099) climate
 502 conditions in each SLR scenario (in yellow-red scale) and the future ensemble mean distribution
 503 of non-operability hours (thick red line??in red).

504

505

506 One additional way to summarize and compare the results obtained is displayed in Table 1. Each
 507 of the present and future distributions of non-operability hours is fitted to a lognormal distribution.
 508 The mean, standard deviation and coefficient of variation are calculated and shown in the table. In
 509 both Areas 1 and 2, the future mean values for non-operability hours are drastically increased (from
 510 198.90 to 332.13 in Area 1 and from 313.62 to 475.14 in Area 2) due to a mean SLR of 0.257 m
 511 by 2050 and 0.634 m by 2100. The latter increase is due to non-linear interactions between waves
 512 and sea level, and changes in the reflection coefficients associated to SLR. Regarding the
 513 nondimensional coefficient of variation, the uncertainty associated with non-operability hours
 514 increases from about 1.3 % (0.0132 in Area 1 and 0.0129 in Area 2) under current in the present
 515 conditions, to around 10 % (0.1163 in Area 1 and 0.1044 in Area 2) in the future ones. These
 516 results differ from the future SLR coefficient of variations (26.7% by 2050 and 31.1% by 2100),
 517 indicating that the magnitude of the SLR uncertainties are reflected to in a lower degree in the
 518 magnitude of the uncertainty of non-operability hours.

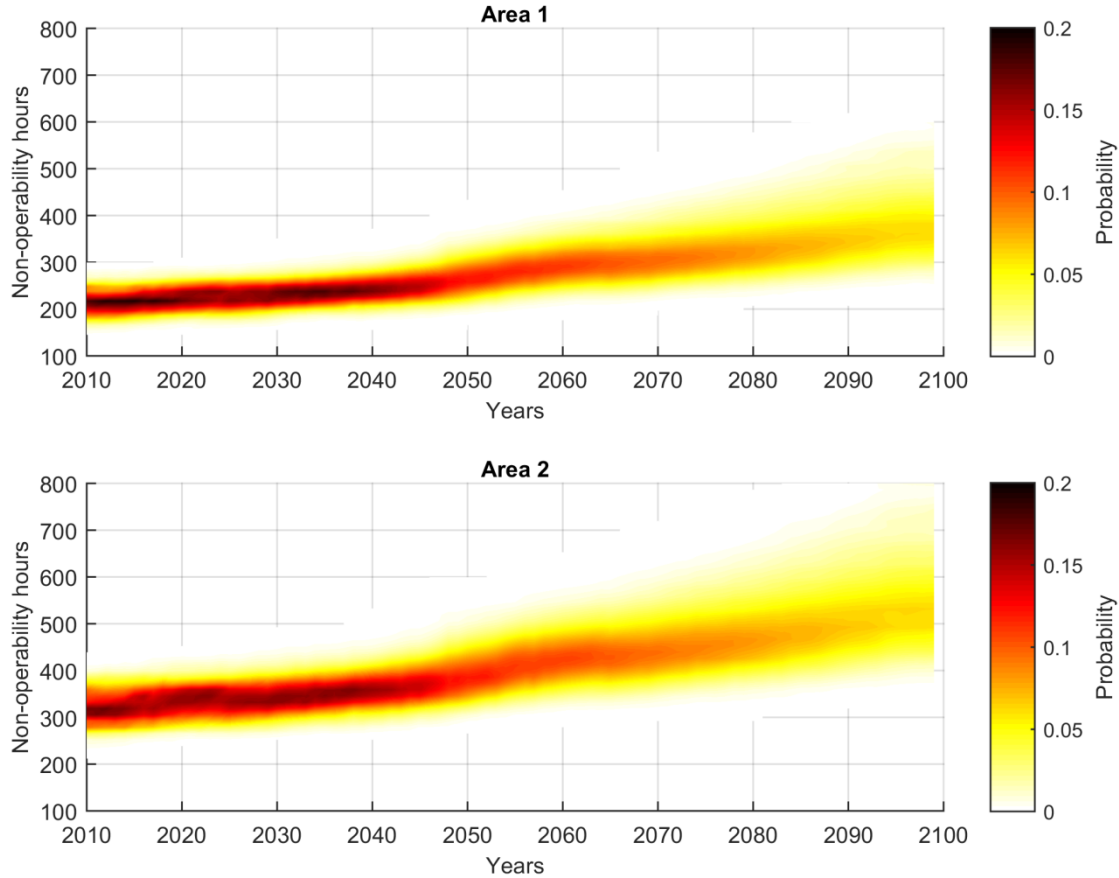
	RCP8.5 SLR (m)		Non-operability (hours)			
			Area 1		Area 2	
	2050	2100	Present	Future (2050-2100)	Present	Future (2050-2100)
Mean	0.257	0.634	198.90	332.13	313.62	475.14
Std	0.069	0.197	2.625	38.61	4.057	49.604
CV (std/mean)	0.267	0.311	0.0132	0.1163	0.0129	0.1044

519 Table 1: Mean, Standard Deviation and Coefficient of Variation of the lognormal distribution of
520 2050 SLR and 2100 SLR predictions? and the lognormal distribution of the non-operability hours
521 for the present and future period in Areas 1 and Area-2.

522

523 ~~The~~ non-operability hours during the useful life of the infrastructure/port taking into account
524 climate change ~~washas been~~ calculated along the 21st century adding the evolution of the SLR to
525 the hourly time series of sea level. In the previous analysis of the impact of climate change in the
526 port's operability, future ~~of~~ non-operability hours ~~wereare~~ calculated for a useful life of 50 years,
527 from 2050 to 2100, to obtain more significant changes. However, ~~the~~ assessment of port operability
528 should be ~~adjustedfit~~ to the projected useful life of the infrastructure, ~~as of starting at the moment~~
529 ~~of~~ its construction. Figure 12 shows the interannual variability of the ensemble's mean probability
530 of non-operability hours from 2010 to 2099 in Areas 1 and Area-2 ~~based on from~~ the ten SLR
531 scenarios. ~~First, the empirical distribution of non-operability hours of non-operability was has been~~
532 ~~calculated on a yearly basis every year~~ for each of the 10 RCP8.5 SLR scenarios considered. ~~The~~
533 ~~m~~Mean sea level rise rates ~~werehave been~~ determined fitting a second order polynomial to the
534 deciles from ~~the~~ local SLR lognormal distribution in 2025, 2050 and 2100. Afterwards, the
535 ensemble mean distribution of non-operability hours ~~was has been~~ calculated every year. An
536 average moving mean of ten years ~~washas been~~ applied. A linear trend of the mean hours of non-
537 operability along the 21st century can be observed in Figure 12 (e.g., downtime increases from
538 320 hours in 2010 to 510 hours in 2100). The dispersion of the empirical density distribution rises
539 along the 21st century due to a broader uncertainty of the SLR scenarios as the horizon increases.
540 At the beginning of the 21st ~~XXI~~ century, the SLR distribution spread ~~wasis~~ limited which ~~it~~ is
541 reflected in a narrow ensemble mean distribution of non-operability hours (i.e., high probability
542 centered in the mean value). However, the SLR distribution ~~is~~ broadened along the 21st century,
543 ~~increasing -which makes~~ the ensemble mean distribution of hours of non-operability ~~wider~~ (e.g.,
544 downtime hours vary from 290 to 400 hours in 2010 and from around 400 to 800 in 2100). An
545 average moving mean of ten years ~~has been~~ applied. It can be observed not only how the mean
546 hours of non-operability increases during the 21st century, also the dispersion of the empirical
547 density distribution rises along the 21st century due to a broader uncertainty of the SLR scenarios
548 as the horizon increases. ~~Changes in The changes of hours of~~ non-operability hour values are more

549 significant after 2050 due to a more pronounced acceleration of SLR as of ~~from~~ the second half
550 of the 21st century.



551

552 **Figure 12.** Interannual ensemble mean probability of non-operability hours from 2010 to 2099 in
 553 Area 1 and Area2 taking into account the increase in SLR uncertainty along the 21st century.

554

555 **5 Summary and conclusions**

556 A hybrid statistical-dynamical framework was developed with two main purposes: 1) to provide
 557 a probabilistic evaluation of port operability to assess ensure the a minimum level of downtime
 558 of the port; 2) -to introduce climate change in the assessment of port operability during its useful
 559 life.

560 The methodology is strongly dependent on the multivariate nature of climate drivers of wave
 561 agitation such as the combination of waves and sea levels and the availability of these forcings
 562 outside the port. Therefore, the following requirements should be met-is required: 1) the use of a
 563 stochastic generator to model the dependence between multivariate conditions; 2) the application
 564 of a numerical modelling approach to propagate wave offshore conditions inside the port.

565 HenceFor said reasons, the methodology includes: 1) A weather generator based on WTs to take
 566 into account future climate variability through WT probability changes linked to changes in
 567 climate drivers (waves and storm surges); 2) A metamodel based on a catalog of wave propagations

568 and a multidimensional non-linear interpolation to reconstruct hourly significant wave height time
569 series inside the port with ~~an similar~~ accuracy similar to that of the numerical simulations.

570 The ~~study~~ case ~~study was~~ is focused on port operability due to wave agitation. The methodology
571 allows to transfer ~~inside the port~~ thousands of synthetic time series ~~of~~ present ~~climate~~ and ~~in the~~
572 future climate conditions inside the port in order to carry out a probabilistic analysis of port
573 operability. Future changes ~~in~~ non-operability are expressed including both uncertainties
574 associated with marine conditions outside the port and SLR. Climate induced changes in waves
575 and storm surge are considered to be negligible due to the projections obtained in the study area.
576 Uncertainty of forcing conditions outside the port ~~was~~ quantified through the use of a weather
577 generator that allows to generate synthetic time series. SLR uncertainty ~~was~~ introduced equally
578 by sampling its probability distribution in several horizons, ~~while~~ ~~and~~ hourly SLR time series
579 ~~are~~ were added to the synthetic sea level fluctuations to define the future forcing conditions outside
580 the port. SLR uncertainty ~~was~~ integrated in the future non-operability evaluation joining the
581 contribution of each sampled SLR scenario with its corresponding probability.

582 Obtaining the future distribution of non-operability hours allows calculating the future probability
583 associated with the non-operability exceedance hours threshold established in ports design
584 recommendations (i.e. ROM 3.1-99, [401]) ~~during their~~ ~~for its~~ useful life. The proposed hybrid
585 methodology produces this very useful and relevant outcome to define a specific acceptable
586 operability risk and can be used as a design criteria ~~on~~ ~~in~~ ~~of~~ ~~a~~ new coastal infrastructures or for
587 climate change adaptation plans.

588 Although, for this specific pilot case, climate induced changes on waves and storm surges, have
 589 been neglected due to ~~their~~ small values, non-linear feedbacks induced by SLR that may produce
 590 an amplification of wave conditions in shallow waters [424] have been introduced in the wave
 591 agitation modeling. Future hourly sea conditions are transformed from the harbor's entrance to
 592 inside the port considering the non-linearities between tides, surges, waves and SLR. Changes in
 593 the reflection coefficient inside the port due to changes in sea level have also been implemented
 594 in the ~~wave agitation~~ simulation ~~of wave agitation~~.

595 The proposed methodology presents several limitations. The synthetic marine conditions are
 596 generated without modelling ~~the dependence~~ time structure ~~dependence~~, which would allow
 597 ~~performing to perform~~ an analysis of ~~the non-operability's~~ persistence. Besides, this version of the
 598 climate emulator is not useful for the analysis of extreme conditions. ~~S~~The synthetic extreme
 599 events are not time independent and their frequency could be overestimated. Nevertheless, our
 600 objective ~~wasis~~ focused on port operability which ~~shoulda~~ not be conditioned by extreme events.

601 The methodology presented can be extended ~~to for~~ further applications such as coastal
 602 infrastructure reliability or operability for other functional parameters or marine operations by
 603 tailoring the weather generator and ~~a~~ selecting the most appropriate numerical model.

604

605 Acknowledgments

606 P. C. and C. I. acknowledge the support of the Spanish Ministerio de Economía y Competitividad
 607 (MINECO) and ~~the~~ European Regional Development Fund (FEDER) under Grant BIA2015-
 608 70644-R (MINECO/FEDER, UE).

609 References

- 610 [1] Becker, A., Inoue, S., Fischer, M., Schwegler, B. (2012). Climate change impacts on
 611 international seaports: Knowledge, perceptions, and planning efforts among port administrators
 612 Climatic Change, 110 (1-2), pp. 5-29.
- 613 [2] Chhetri, P., Corcoran, J., Gekara, V., Maddox, C., McEvoy, D. (2014): Seaport resilience to
 614 climate change: mapping vulnerability to sea-level rise, Journal of Spatial Science, DOI:
 615 10.1080/14498596.2014.943311.
- 616 [3] Becker, A.H., Acciaro, M., Asariotis, R., Cabrera, E., Cretegnny, L., Crist, P., Esteban, M.,
 617 Mather, A., Messner, S., Naruse, S., Ng, A.K.Y., Rahmstorf, S., Savonis, M., Song, D.-W., Stenek,
 618 V., Velegrakis, A.F. (2013). A note on climate change adaptation for seaports: A challenge for
 619 global ports, a challenge for global society. Climatic Change, 120 (4), pp. 683-695.
- 620 [4] McEvoy, D, Mullett, J, Millin, S, Scott, H & Trundle, A 2013, Understanding future risks to
 621 ports in Australia. Work Package 1 of Enhancing the resilience of seaports to a changing climate
 622 report series, National Climate Change Adaptation Research Facility, Gold Coast, 77 pp.
- 623 [5] Nicholls, R. J., Hanson, S., Herweijer, C., Patmore, N., Hallegatte, S., Corfee-Morlot, J.,
 624 Chateau, J. and Wood, R.M. (2008). Ranking port cities with high exposure and vulnerability to
 625 climate extremes: exposure estimates. Environment Working Papers no.1, OECD.

- 626 [6] Sánchez-Arcilla, A., Sierra, J.P., Brown, S., Casas-Prat, M., Nicholls, R.J., Lionello, P., Conte,
627 D. (2016). A review of potential physical impacts on harbours in the Mediterranean Sea under
628 climate change. *Regional Environmental Change*, 16 (8), pp. 2471-2484.
- 629 [7] Sierra, J.P., Casas-Prat, M., Virgili, M., Mösso, C., Sánchez-Arcilla, A. (2015). Impacts on
630 wave-driven harbour agitation due to climate change in Catalan ports. *Natural Hazards and Earth
631 System Sciences*, 15 (8), pp. 1695-1709.
- 632 [8] Sierra, J.P., Genius, A., Lionello, P., Mestres, M., Mösso, C., Marzo, L. (2017). Modelling the
633 impact of climate change on harbour operability: The Barcelona port case study. *Ocean
634 Engineering*, 141, pp. 64-78.
- 635 [9] Camus, P., Losada, I.J., Izaguirre, C., Espejo, A., Menéndez, M., Pérez, J. (2017). Statistical
636 wave climate projections for coastal impact assessments. *Earth's Future*, 5 (9), pp. 918-933.
- 637 [10] Ranasinghe, R., 2016. Assessing climate change impacts on open sandy coasts: a review.
638 *Earth-Sci. Rev.* 160, 320–332.
- 639 [11] Gouldby, B., Méndez, F.J., Guanche, Y., Rueda, A., Mínguez, R., 2014. A methodology for
640 deriving extreme nearshore sea conditions for structural design and flood risk analysis. *Coastal
641 Eng.* 88, 15–26.
- 642 [12] Camus, P., F. J. Mendez, R. Medina (2011). A hybrid efficient method to downscale wave
643 climate to coastal areas. *Coastal Engineering*, 58 (9), 851-862.
- 644 [13] Gouldby, B., Wyncoll, D., Panzeri, M., Franklin, M., Hunt, T., Hames, D., Tozer, N., Hawkes,
645 P., Dornbusch, U., Pullen, T. (2017). Multivariate extreme value modelling of sea conditions
646 around the coast of England. *Proceedings of the Institution of Civil Engineers: Maritime
647 Engineering*, 170 (1), pp. 3-20.
- 648 [14] López, I., López, M., Iglesias, G. (2015). Artificial neural networks applied to port operability
649 assessment. *Ocean Eng.* 109, 298–308.
- 650 [15] ROM 0.0 (2001) General Procedure & Requirements for Design of Maritime & Harbour
651 Structures (Part I); Puertos del Estado. www.puertos.es ISBN 84-88975-31-7
- 652 [16] Heffernan, J.E., Tawn, J.A., 2004. A conditional approach for multivariate extreme values
653 (with discussion). *J. R. Statist. Soc.* 66 (3), 497–546.
- 654 [17] Wahl, T., C. Mudersbach, and J. Jensen (2012), Assessing the hydrodynamic boundary
655 conditions for risk analyses in coastal areas: A multivariate statistical approach based on Copula
656 functions, *Nat. Hazards Earth Syst. Sci.*, 12(2), 495–510.
- 657 [18] Corbella, S., and D. D. Stretch (2013), Simulating a multivariate sea storm using Archimedean
658 copulas, *Coastal Eng.*, 76, 68–78.
- 659 [19] Wahl, T., Plant, N.G., Long, J.W., 2016. Probabilistic assessment of erosion and flooding risk
660 in the northern Gulf of Mexico. *J. Geophys. Res. Oceans* 121. doi: 10.1002/2015JC011482.
- 661 [20] Rueda, A., Camus, P., Tomás, A., Vitousek, S., Méndez, F.J. (2016). A multivariate extreme
662 wave and storm surge climate emulator based on weather patterns. *Ocean Modelling*, 104, 242-
663 251.
- 664 [21] Guedes Soares, C. and C. Cunha (2000). Bivariate autoregressive models for the time series
665 of significant wave height and mean period. *Coastal Engineering* 40, 297–311.

- 666 [22] Solari, S., van Gelder, P.H., (2012). On the use of vector autoregressive VAR and regime
667 switching VAR models for the simulation of sea and wind state parameters. In: Carlos Guedes
668 Soares, et al. (Eds.), *Marine Technology and Engineering*. Taylor & Francis Group, London,
669 pp.217–230.
- 670 [23] Solari, S., Losada, M.T. (2016). Simulation of non-stationary wind speed and direction time
671 series. *Journal of Wind Engineering and Industrial Aerodynamics*, 149, pp. 48-58.
- 672 [24] Saha, S., S. Moorthi, X. Wu, J. Wang, S. Nadiga, P. Tripp, D. Behringer, Y.T. Hou, H.Y.
673 Chuang, M. Iredell, M. Ek, J. Meng, R. Yang, M.P.n. Mendez, H. van den Dool, Q. Zhang, Wang,
674 M. Chen and E. Becker (2014), The NCEP Climate Forecast System Version 2. *Journal of Climate*
675 27, 2185-2208, doi: 10.1175/JCLI-D-12-00823.1.
- 676 [25] Camus, P., Méndez, F.J., Medina, R., Tomás, A., Izaguirre, C. (2013). High resolution
677 downscaled ocean waves (DOW) reanalysis in coastal areas. *Coastal Engineering*, 72, 56-68.
- 678 [26] Reguero, B.G., Menéndez, M., Méndez, F.J., Mínguez, R., Losada, I.J. (2012). A Global
679 Ocean Wave (GOW) calibrated reanalysis from 1948 onwards *Coastal Engineering*, 65, pp. 38-
680 55.
- 681 [27] Menendez M, García-Díez M, Fita L, Fernández J, Méndez FJ, Gutiérrez JM (2013) High-
682 resolution sea wind hindcasts over the Mediterranean area. *Clim Dyn.* doi:10.1007/s00382-013-
683 1912-8
- 684 [28] Cid A, Castanedo S, Abascal AJ, Menéndez M, Medina R (2014) A high resolution hindcast
685 of the meteorological sea level component for Southern Europe: the GOS dataset. *Clim Dyn.*
686 doi:10.1007/s00382-013-2041-0.
- 687 [29] Slangen, A.B.A., M. Carson and C.A. Katsman (2014), Modelling twenty-first century
688 regional sea-level changes, *Clim Change*, doi:10.1007/s10584-014-1080-9.
- 689 [30] GIOC, 2000. MSP: A Finite element model for wave agitation in ports. Technical Report and
690 User Manual. Universidad de Cantabria (in Spanish).
- 691 [31] Cannon, A. J. (2012), Regression-guided clustering: A semisupervised method for circulation-
692 to-environment synoptic classification, *J.Appl.Meteorol. Climatol.*, 51, 185–190.
693 <https://doi.org/10.1175/jamc-d-11-0155.1>.
- 694 [32] Solari, S., Losada, M.A. (2012b). Unified distribution models for met-ocean variables:
695 Application to series of significant wave height. *Coastal Engineering*, 68, pp. 67-77.
- 696 [33] Toimil, A., Losada, I.J., Camus, P., Díaz-Simal, P. (2017). Managing coastal erosion under
697 climate change at the regional scale. *Coastal Engineering*, 128, pp. 106-122.
- 698 [34] Camus, P., Menéndez, M., Méndez, F.J., Izaguirre, C., Espejo, A., Cánovas, V., Pérez, J.,
699 Rueda, A., Losada, I.J., Medina, R., 2014. A weather-type statistical downscaling framework for
700 ocean wave climate. *Journal of Geophysical Research*, DOI: 10.1002/2014JC010141
- 701 [35] Perez, J., Menendez, M., Camus, P., Mendez, F.J., Losada, I.J. (2015). Statistical multi-model
702 climate projections of surface ocean waves in Europe. *Ocean Modelling*, 96, 161-170.
- 703 [36] Quinn, N., P. D. Bates, and M. Siddall (2013). The contribution to future flood risk in the
704 Severn Estuary from extreme sea level rise due to ice sheet mass loss, *J. Geophys. Res. Oceans*,
705 118, 5887–5898, doi:10.1002/jgrc.20412.

- 706 [37] Bamber, J. L., and W. P. Aspinall (2013), An expert judgement assessment of future sea level
707 rise from the ice sheets, *Nat. Clim. Change*, 3, 424–427, doi:10.1038/nclimate1778.
- 708 [38] IPCC 2013. *Climate Change 2013: The Physical Science Basis*. Contribution of Working
709 Group I to the Fifth Assessment Report of the Intergovernmental Panel on Climate Change
710 [Stocker, T.F., D. Qin, G.-K. Plattner, M. Tignor, S.K. Allen, J. Boschung, A. Nauels, Y. Xia, V.
711 Bex and P.M. Midgley (eds.)].
- 712 [39] Diaz-Hernandez, G., Mendez, F.J., Losada, I.J., Camus, P., Medina, R. (2015). A nearshore
713 long-term infragravity wave analysis for open harbours. *Coastal Engineering*, 97, 78-90.
- 714 [40] Rippa, S., 1999. An algorithm for selecting a good value for the parameter c in radial basis
715 function interpolation. *Advances in Computational and Mathematical* 11, 193–210
- 716 [41] ROM 3.1 (1999) *Maritime Port Configuration Design: Approach channel & Harbour basin;*
717 *Puertos del Estado* www.puertos.es ISBN 84-88975-52-X
- 718 [42] Arns, A., S. Dangendorf, J. Jensen, S. Talke, J. Bender, and C. Pattiaratchi (2017). Sea-level
719 rise induced amplification of coastal protection design heights, *Sci. Rep.*, 7, art. no. 40171.
720 <https://doi.org/10.1038/srep40171>.
- 721